

Multi- τ signatures at the LHC in the two Higgs doublet model

Shinya Kanemura,^{1,*} Koji Tsumura,^{2,†} and Hiroshi Yokoya^{2,3,‡}

¹*Department of Physics, The University of Toyama, Toyama 930-8555, Japan*

²*Department of Physics and Center for Theoretical Sciences,*

National Taiwan University, Taipei 10617, Taiwan

³*National Center for Theoretical Sciences,*

National Taiwan University, Taipei 10617, Taiwan

(Dated: November 6, 2018)

Abstract

A detailed simulation study is performed for multi- τ signatures at the Large Hadron Collider, which can be used to probe additional Higgs bosons with lepton-specific Yukawa interactions. Such an extended Higgs sector is introduced in some of new physics models at the TeV scale. We here consider the two Higgs doublet model with the Type-X Yukawa interaction, where nonstandard Higgs bosons predominantly decay into tau leptons. These extra Higgs bosons can be pair produced via s -channel gauge boson mediation at hadron colliders; $q\bar{q} \rightarrow Z^* \rightarrow HA$ and $q\bar{q}' \rightarrow W^{\pm*} \rightarrow HH^\pm (AH^\pm)$, where H , A and H^\pm are CP-even, odd and charged Higgs bosons, respectively. Consequently, multi- τ originated signals appear in the final state as a promising signature of such a model. We find that the main background can be considerably reduced by requiring the high multiplicity of leptons and tau-jets with appropriate kinematical cuts in the final state. Thus, assuming the integrated luminosity of a hundred of inverse fb, the excess can be seen in various three- and four-lepton channels. With the integrated luminosity of thousands of inverse fb, the determination of the mass as well as ratios of leptonic decay branching ratios of these Higgs bosons would also be possible.

PACS numbers: 12.60.Fr, 14.60.Fg, 14.80.Cp

Keywords: Higgs boson, tau lepton, hadron colliders

*Electronic address: kanemu@sci.u-toyama.ac.jp

†Electronic address: ko2@phys.ntu.edu.tw

‡Electronic address: hyokoya@hep1.phys.ntu.edu.tw

I. INTRODUCTION

The $SU(3)_C \times SU(2)_L \times U(1)_Y$ gauge structure of the standard model (SM) for elementary particles has been tested precisely [1]. A missing piece is the Higgs boson, which is responsible for electroweak symmetry breaking and mass generation mechanisms for all SM particles. It is expected that the Higgs boson will be discovered at the Large Hadron Collider (LHC) in near future. The LHC is also searching for the evidence of new physics beyond the SM [2, 3]. The LHC has already clarified the absence of light new colored particles; e.g., squarks and gluinos in the supersymmetric theories [2], or forth generation quarks [3]. However, a light particle without strong interactions has not been ruled out yet by the LHC data because of small production cross sections.

The Higgs sector is totally unknown, since no Higgs boson has been discovered yet [4–6]. In the SM, only one scalar iso-doublet field is introduced to spontaneously break the electroweak gauge symmetry. However, since there is no reason for the Higgs sector with only one doublet, there is a possibility of non-minimal Higgs sectors. There are two important experimental constraints on extended Higgs sectors; i.e., the flavor changing neutral current (FCNC) and the electroweak rho parameter. In the SM, these constraints are automatically satisfied: FCNC is suppressed by the Glashow-Iliopoulos-Maiani mechanism, and the rho parameter is predicted to be unity at the tree level due to the custodial $SU(2)$ symmetry. On the other hand, non-minimal Higgs sectors suffer from both of them in general. It is known that in the Higgs sector with only doublets, the rho parameter is predicted to be unity at the tree level, while Higgs models with higher representations such as those with triplet fields predict the rho parameter to be different values from unity. Therefore, two Higgs doublet models (THDMs) would be a simplest viable extension of the SM. However, in the THDM the most general Yukawa interaction predicts FCNC at the tree level, because both the doublet couples to a fermion so that the mass matrix and the Yukawa matrix cannot be diagonalized simultaneously. In order to avoid this, a discrete symmetry may be introduced under which different properties are assigned to each scalar doublet [7]. Under this symmetry, each fermion couples with only one scalar doublet, and hence there are no FCNC at the tree level even in the THDM.

There are four types of Yukawa interactions depending on the Z_2 -charge assignments; i.e., Type-I, II, X and Y. Type-II is the most familiar type of Yukawa interactions in the THDM, which is the Higgs sector of the minimal supersymmetric standard model (MSSM). Another interesting possibility would be the Type-X THDM, where one Higgs doublet couples with quarks and the other does with leptons [8–10]. The Type-X THDM can appear in the Higgs sector of a gauged extension of the Type-III seesaw model [11], the model of three-loop seesaw with electroweak baryogenesis [12] and a model for positron cosmic ray anomaly [13]. In the SM-like limit, where only one of the CP-even Higgs bosons couples to the gauge bosons, the Yukawa couplings of the other Higgs bosons tend to be lepton-specific. Since Yukawa coupling constants are proportional to the mass of fermions, these extra Higgs bosons predominantly decay into tau leptons for the wide range of the parameter space [9].

The tau lepton has a relatively short lifetime as compared with the muon. It decays into

lighter leptons and/or hadrons with neutrinos in the detector. The decay products always produce missing energies, which make event reconstructions rather complicated. However, for an energetic tau lepton, the missing momentum from its decay tends to be oriented to the same direction of the charged track [14]. Therefore, the tau lepton momentum can be approximately reconstructed by using the collinear approximation [14]. Furthermore, the decay of the tau lepton is correlated by its polarization, which can be used to separate leptonic decays from hadronic decays [15].

In this paper, we study multi- τ signatures at the LHC in the lepton-specific THDM in the SM-like limit. Masses of extra Higgs bosons can be of the order of a hundred GeV under the $B_s \rightarrow X_s \gamma$ results. Then the gluon fusion mechanism for such extra Higgs bosons is suppressed at hadron colliders. In this case, extra Higgs bosons can be pair produced; $q\bar{q} \rightarrow Z^* \rightarrow HA$ and $q\bar{q}' \rightarrow W^{\pm*} \rightarrow HH^\pm (AH^\pm)$, where H , A and H^\pm are CP-even, odd and charged Higgs bosons, respectively. Produced Higgs bosons mainly decay into tau leptons because the Yukawa coupling constant is proportional the fermion mass. These characteristic decay modes can be observed in multi- τ signatures at the LHC. We perform detailed simulation studies for the pair production of the extra Higgs bosons where they subsequently decay into multi- τ states. It is found that the main background can be considerably reduced by requiring the high multiplicity of leptons and tau-jets with appropriate kinematical cuts in the final state. Assuming the integrated luminosity of a hundred of inverse fb, the excess can be seen in various three- and four-lepton channels.

This paper is organized as follows. In Sec. II, we summarize the Type-X THDM and give basic constraints on the model. The simulation studies of multi- τ signatures at the LHC in the lepton-specific THDM are presented in Sec. III. Summary and discussions are given in Sec. IV.

II. THE MODEL AND CONSTRAINTS

The Higgs potential of the THDM is defined as [16, 17]

$$\begin{aligned} \mathcal{V}^{\text{THDM}} = & +m_1^2 \Phi_1^\dagger \Phi_1 + m_2^2 \Phi_2^\dagger \Phi_2 - m_3^2 (\Phi_1^\dagger \Phi_2 + \Phi_2^\dagger \Phi_1) + \frac{\lambda_1}{2} (\Phi_1^\dagger \Phi_1)^2 + \frac{\lambda_2}{2} (\Phi_2^\dagger \Phi_2)^2 \\ & + \lambda_3 (\Phi_1^\dagger \Phi_1) (\Phi_2^\dagger \Phi_2) + \lambda_4 (\Phi_1^\dagger \Phi_2) (\Phi_2^\dagger \Phi_1) + \frac{\lambda_5}{2} [(\Phi_1^\dagger \Phi_2)^2 + (\Phi_2^\dagger \Phi_1)^2], \end{aligned} \quad (1)$$

where $\Phi_i (i = 1, 2)$ are the Higgs doublets with hypercharge $Y = 1/2$. A softly broken Z_2 symmetry is imposed in the model to forbid FCNC at the tree level, under which the Higgs doublets are transformed as $\Phi_1 \rightarrow +\Phi_1$ and $\Phi_2 \rightarrow -\Phi_2$ [7]. The soft-breaking parameter m_3^2 and the coupling constant λ_5 are complex in general. We here take them to be real assuming that CP is conserved in the Higgs sector.

The Higgs doublets can be written in terms of the component fields as

$$\Phi_i = \begin{pmatrix} i\omega_i^+ \\ \frac{1}{\sqrt{2}}(v_i + h_i - iz_i) \end{pmatrix}, \quad (2)$$

where the vacuum expectation values (VEVs) v_1 and v_2 satisfy $\sqrt{v_1^2 + v_2^2} = v \simeq 246$ GeV and

	Φ_1	Φ_2	u_R	d_R	ℓ_R	Q_L, L_L
Type-I	+	-	-	-	-	+
Type-II	+	-	-	+	+	+
Type-X	+	-	-	-	+	+
Type-Y	+	-	-	+	-	+

TABLE I: Variation in charge assignments of the softly broken Z_2 symmetry [9].

$\tan \beta \equiv v_2/v_1$. The mass eigenstates are obtained by rotating the component fields as

$$\begin{pmatrix} h_1 \\ h_2 \end{pmatrix} = \mathbf{R}(\alpha) \begin{pmatrix} H \\ h \end{pmatrix}, \quad \begin{pmatrix} z_1 \\ z_2 \end{pmatrix} = \mathbf{R}(\beta) \begin{pmatrix} z \\ A \end{pmatrix}, \quad \begin{pmatrix} \omega_1^+ \\ \omega_2^+ \end{pmatrix} = \mathbf{R}(\beta) \begin{pmatrix} \omega^+ \\ H^+ \end{pmatrix}, \quad (3)$$

where ω^\pm and z are the Nambu-Goldstone bosons, h, H, A and H^\pm are respectively two CP-even, one CP-odd and charged Higgs bosons, and

$$\mathbf{R}(\theta) = \begin{pmatrix} \cos \theta & -\sin \theta \\ \sin \theta & \cos \theta \end{pmatrix}. \quad (4)$$

The eight parameters $m_1^2 - m_3^2$ and $\lambda_1 - \lambda_5$ are replaced by the VEV v , the mixing angles α and $\tan \beta$, the Higgs boson masses m_h, m_H, m_A and m_{H^\pm} , and the soft Z_2 breaking parameter $M^2 = m_3^2/(\cos \beta \sin \beta)$. The coupling constants of the CP-even Higgs bosons with weak gauge bosons hVV and HVV ($V = W, Z$) are proportional to $\sin(\beta - \alpha)$ and $\cos(\beta - \alpha)$, respectively. When $\sin(\beta - \alpha) = 1$, only h couples to the gauge bosons while H decouples. We call this limit as the SM-like limit where h behaves as the SM Higgs boson [18, 19].

Assuming the discrete symmetry (see TABLE I), there can be four types of Yukawa interactions in the THDM, i.e., Type-I, II, X and Y [8, 9];

$$\mathcal{L}_{\text{yukawa}}^{\text{THDM}} = -\bar{Q}_L Y_u \tilde{\Phi}_u u_R - \bar{Q}_L Y_d \Phi_d d_R - \bar{L}_L Y_\ell \Phi_\ell \ell_R + \text{H.c.}, \quad (5)$$

where Φ_f ($f = u, d$ or ℓ) is either Φ_1 or Φ_2 . In the Type-I THDM, all fermions obtain their masses from the VEV of Φ_2 . In the Type-II THDM, masses of up-type quarks are generated by Φ_2 while those of down-type quarks and charged leptons are acquired by Φ_1 . The Higgs sector of the MSSM is a special THDM, whose Higgs potential is determined by gauge coupling constants and whose Yukawa interaction is of Type-II [16]. In the Type-X Yukawa interaction, all quarks couple to Φ_2 while charged leptons couple to Φ_1 . Remaining one is referred to the Type-Y. The Yukawa interactions are expressed in terms of mass eigenstates of the Higgs bosons as

$$\begin{aligned} \mathcal{L}_{\text{yukawa}}^{\text{THDM}} = & - \sum_{f=u,d,\ell} \left[+\frac{m_f}{v} \xi_h^f \bar{f} f h + \frac{m_f}{v} \xi_H^f \bar{f} f H - i\frac{m_f}{v} \xi_A^f \bar{f} \gamma_5 f A \right] \\ & - \left\{ +\frac{\sqrt{2}V_{ud}}{v} \bar{u} [+m_u \xi_A^u P_L + m_d \xi_A^d P_R] d H^+ + \frac{\sqrt{2}m_\ell \xi_A^\ell}{v} \bar{\nu}_L \ell_R H^+ + \text{H.c.} \right\}, \quad (6) \end{aligned}$$

where $P_{L(R)}$ are projection operators for left-(right-)handed fermions, and the factors ξ_φ^f are listed in TABLE II.

	ξ_h^u	ξ_h^d	ξ_h^ℓ	ξ_H^u	ξ_H^d	ξ_H^ℓ	ξ_A^u	ξ_A^d	ξ_A^ℓ
Type-I	c_α/s_β	c_α/s_β	c_α/s_β	s_α/s_β	s_α/s_β	s_α/s_β	$\cot\beta$	$-\cot\beta$	$-\cot\beta$
Type-II	c_α/s_β	$-s_\alpha/c_\beta$	$-s_\alpha/c_\beta$	s_α/s_β	c_α/c_β	c_α/c_β	$\cot\beta$	$\tan\beta$	$\tan\beta$
Type-X	c_α/s_β	c_α/s_β	$-s_\alpha/c_\beta$	s_α/s_β	s_α/s_β	c_α/c_β	$\cot\beta$	$-\cot\beta$	$\tan\beta$
Type-Y	c_α/s_β	$-s_\alpha/c_\beta$	c_α/s_β	s_α/s_β	c_α/c_β	s_α/s_β	$\cot\beta$	$\tan\beta$	$-\cot\beta$

TABLE II: The mixing factors in each type of Yukawa interactions in Eq. (6) [9].

Experimental constraints on masses of Higgs bosons H , A , H^\pm in THDMs depend on the type of the Yukawa interaction. Masses of neutral bosons have been bounded by LEP experiment to be $m_H > 92.8$ GeV and $m_A > 93.4$ GeV in the MSSM (Type-II THDM with additional relations) [1]. At the LHC, neutral Higgs bosons can be produced via gluon fusion $gg \rightarrow \phi^0$ [20] where we define $\phi^0 = H, A$, associated production with heavy quarks $pp \rightarrow t\bar{t}\phi^0$, $b\bar{b}\phi^0$ [21] and the weak boson mediated processes $pp \rightarrow Z^* \rightarrow HA$ [18] and $pp \rightarrow W^{\pm*} \rightarrow \phi^0 H^\pm$ [22]. For the large $\tan\beta$ region, stronger mass bounds can be obtained from these production processes at the Tevatron and the LHC [23, 24]. However, if the Yukawa interactions of H and A are quarkophobic which is realized in the wide parameter space in the Type-X THDM, these Higgs bosons are less constrained. The search for such Higgs bosons at the LEP experiments is found in Ref. [25]. On the other hand, direct search bounds on charged Higgs boson mass has also been set by LEP experiments as $m_{H^\pm} > 79.3$ GeV by assuming $\mathcal{B}(H^+ \rightarrow c\bar{s}) + \mathcal{B}(H^+ \rightarrow \tau^+\nu) = 1$ [26]. Further stronger bound can be obtained in the Type-II(Y) THDM [8, 27] from the $B_s \rightarrow X_s\gamma$ results as $m_{H^\pm} > 295$ GeV [28]. The observation of $B \rightarrow \tau\nu$ decay also constrains the mass of charged Higgs bosons for the large $\tan\beta$ region [29]. The LHC can also search for charged Higgs bosons in various production processes such as $pp \rightarrow H^+H^-$ [30], $gb \rightarrow tH^-$ [31] and $pp \rightarrow W^\pm H^\mp$ [32]. However, these bounds depend on the types of the Yukawa interactions. Therefore, the relatively light charged Higgs boson is still allowed by experimental data in the Type-I(X) THDM. In the Type-X THDM, the charged Higgs boson mass can be constrained by the leptonic decays of tau leptons [33, 34]. Extra Higgs boson searches in the MSSM (Type-II THDM) have been well studied so far in the literature. Fermiophobic Higgs scenario in the Type-I THDM has also been discussed [35].

In this paper, we focus on the Higgs boson search in the Type-X THDM, which is less constrained by B decay data. In this model, more than 99% of H and A decay into pairs of tau leptons for $\tan\beta \gtrsim 3$ in the SM-like limit; $\sin(\beta - \alpha) = 1$ [9]. The neutral Higgs bosons would be produced in pair by $q\bar{q} \rightarrow Z^* \rightarrow HA$ process at the LHC. These Higgs bosons predominantly decay into a four- τ state, $HA \rightarrow (\tau^+\tau^-)(\tau^+\tau^-)$, which is the characteristic signal of the Type-X THDM. The tau leptons further decay into leptons or hadrons with neutrinos. Consequently, there are several *four-lepton* final states such as $llll$, $ll\ell\tau_h$, $\ell\ell\tau_h\tau_h$, $\ell\tau_h\tau_h\tau_h$ and $\tau_h\tau_h\tau_h\tau_h$ with missing energies, where ℓ denotes an election e or a muon μ , and τ_h is hadronic decay products of the tau lepton. Although the branching ratios of the $\phi^0 \rightarrow \mu^+\mu^-$ decay are not large; namely $\mathcal{B}(\phi^0 \rightarrow \mu^+\mu^-) \sim (m_\mu/m_\tau)^2 \sim 0.35\%$, the $HA \rightarrow (\mu^+\mu^-)(\tau^+\tau^-)$ decay process would also be a clear signature, since the invariant mass of the muon pair has a peak at $M_{\mu\mu} \simeq m_H$ and $M_{\mu\mu} \simeq m_A$. This signature results in $\mu^+\mu^-\ell\ell$, $\mu^+\mu^-\ell\tau_h$ and $\mu^+\mu^-\tau_h\tau_h$ final states. We will give the results for simulations of these signals in the

next section.

As for the charged Higgs boson associated production, the processes $q\bar{q}' \rightarrow W^{\pm*} \rightarrow \phi^0 H^\pm$ would be dominant. For $\tan\beta \gtrsim 2$, more than 99% of charged Higgs bosons decay into a tau lepton with a neutrino and 0.35% does into a muon with a neutrino. Therefore, the characteristic signatures for this process consist of three tau leptons $\phi^0 H^\pm \rightarrow (\tau^+\tau^-)(\tau^\pm\nu)$, one tau lepton with two muons $\phi^0 H^\pm \rightarrow (\mu^+\mu^-)(\tau^\pm\nu)$ or two tau leptons with one muon $\phi^0 H^\pm \rightarrow (\tau^+\tau^-)(\mu^\pm\nu)$. These signals result in the *three-lepton* final states; lll , $ll\tau_h$, $\ell\tau_h\tau_h$ and $\tau_h\tau_h\tau_h$ with the large missing energy. In the next section, we study the collider signature of these final states in details.

III. MULTI- τ SIGNATURES

In this section, we present the results of our simulation study for the multi- τ signatures at the LHC in order to probe the production of neutral and charged Higgs bosons, which predominantly decay into tau leptons and occasionally into muons.

First, we explain the framework of our simulation and event analysis. Second, we present studies for the pair production process of the neutral Higgs bosons. Finally, we present studies for the charged Higgs bosons associated production with the neutral Higgs bosons.

A. Framework for event generation and pre-selection

The signal events are generated by using `MadGraph/MadEvent` [36], where the decay of tau leptons is simulated by using `TAUOLA` [37]. The partonic events are passed to `PYTHIA` [38] for parton showering and hadronization. Initial-state-radiation (ISR) and final-state-radiation (FSR) effects are included. We choose the collision energy to be 14 TeV, and use the `CTEQ6L` parton distribution functions [39]. Throughout this paper, we set the masses of extra Higgs bosons to $m_H = 130$ GeV, $m_A = 170$ GeV and $m_{H^\pm} = 150$ GeV, and take the SM-like limit; $\sin(\beta - \alpha) = 1$. The total cross section for $pp \rightarrow HA$ is estimated to be 53 fb at the tree level [9]. For the charged Higgs boson associated production, $pp \rightarrow \phi^0 H^\pm$, the total cross sections are estimated to be 125 fb for HH^\pm production, and 77 fb for AH^\pm production. These mass splitting among the extra Higgs bosons are allowed by electroweak precision data in the SM-like limit [40, 41]. Background events for VV ($= ZZ$, ZW and WW), $t\bar{t}$ processes where the weak bosons decay leptonically and hadronically, and V +jets ($V = W$ and Z) processes followed by leptonic decays of weak bosons are generated by `PYTHIA`, where the decays of tau leptons are also handled by `TAUOLA`. The total cross sections for these processes are given as 108 pb, 493 pb and 110(30) nb, respectively for VV , $t\bar{t}$ and $W(Z)$ +jets production processes by `PYTHIA`. We ignore K -factor corrections for all the signal and background processes, for simplicity.

First, we perform the pre-selection of the events in various four- and three-lepton channels. In

order to take into account the detector availability, muons and electrons are required to be isolated¹ and have $p_T \geq 15$ GeV and $|\eta| \leq 2.5$, where p_T is the transverse momentum, the pseudorapidity is defined as $\eta = (1/2) \ln[\tan(\theta/2)]$ from the scattering angle θ in the laboratory frame. Those muons and electrons are counted in the events. Then, we construct primal jets from the final state hadrons by anti- k_T algorithm [42] with $R = 0.4$ using the **FastJet** package [43]. Among the constructed primal jets, we identify the tau-jet candidates by the following criteria;

a jet with $p_T \geq 10$ GeV and $|\eta| \leq 2.5$ which contains 1 or 3 charged hadrons in a small cone ($R = 0.15$) centered at the jet momentum direction with the transverse energy deposit to this small cone more than 95% of the jet.

The $R = 0.4$ cone of the primal jet acts as an isolation cone to reduce the mis-tagging probability for non-tau jets. We present an estimation of the tau-tagging efficiency and the mis-tagging probability in Appendix. A. The other jets with $p_T \geq 25$ GeV and $|\eta| \leq 5$ are regarded as a hard jet, which are used to estimate the hard QCD activity of the event. Finally, the missing transverse momentum \vec{p}_T^{miss} is calculated as a negative vector sum of the transverse momentum of visible particles, $\vec{p}_T^{\text{miss}} = -\sum_{\text{vis.}} \vec{p}_T$.

We assume that electric charges of tau-jets are measurable. Using the charges of tau-jets, we require the charge sum of the four leptons in the four-lepton channels to vanish to reduce the contributions from the background with mis-identified tau-jets. After the pre-selection of the signal and background events, we perform further event analysis for each channel.

B. Neutral Higgs boson pair production

Here, we present the results of simulation studies for the neutral Higgs boson pair production process. In the Type-X scenario, this process is characterized by the four-lepton signature, where the leptons can be charged leptons e , μ and also the tau-jet τ_h . There are fifteen kinds of the four-lepton channels in total. For the convenience of our analysis, we divide the leptonic channels into three categories; the channels which contain two or more muons, those which contain two or more tau-jets, and those with two or more electrons. However the last channels are difficult to be utilized due to the limited statistics and the negligibly small branching ratio of the Higgs bosons into electrons.

1. Four-lepton channels with two or more muons

As we have mentioned at the end of Sec. II, the dimuon from the direct decay of the Higgs bosons would be a clear signature in the Type-X THDM. Although the decay branching ratio is

¹ The isolation condition for muons is given by $p_T^{\text{cone}}/p_T^\mu < 0.2$ where p_T^{cone} is the sum of the magnitude of the transverse momentum of the particles inside the $R = 0.4$ cone around the muon. The isolation condition for electrons is given by $p_T^e/p_T^{\text{jet}} > 0.95$, where p_T^{jet} is the transverse momentum of the jet which contains the electron itself. The jet is constructed from the final state hadrons, electrons, photons and non-isolated muons. For our isolation conditions, the finding efficiency of muons is slightly better than that of electrons.

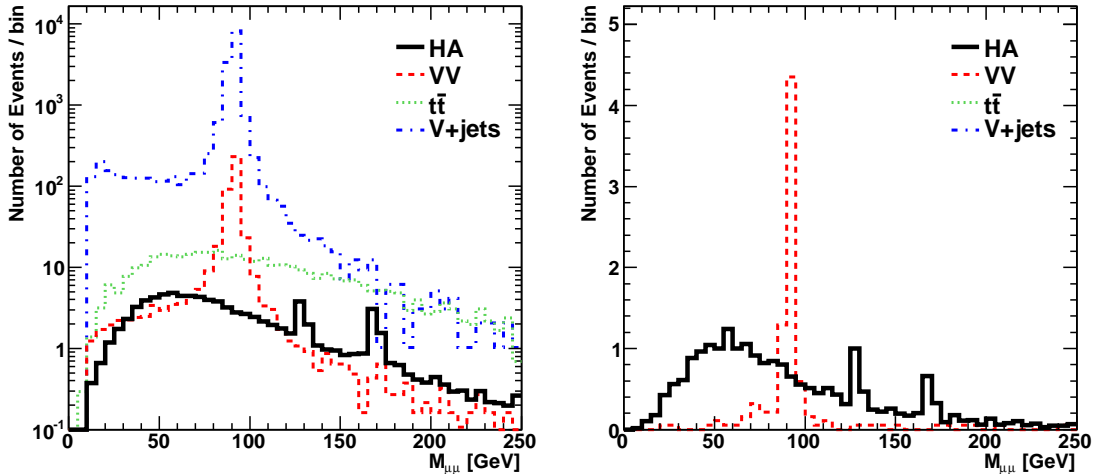


FIG. 1: The dimuon invariant mass distribution for the $2\mu 2\tau_h$ channel after the pre-selection (left) and after the selection cuts before the m_Z -window cut in TABLE III (right). The solid black line is for the signal from HA production, the dashed red line is for the VV production, the dotted green line is for the $t\bar{t}$ production and the dot-dashed blue line is for the V +jets production. In the signal process, $m_H = 130$ GeV and $m_A = 170$ GeV are taken.

only 0.35%, there is no way to ignore this signature. First, we explain the study for the $2\mu 2\tau_h$ channel in detail, and then we comment and summarize the other channels with two or more muons.

After the pre-selection, the obtained numbers of events for the $2\mu 2\tau_h$ channel are 91, 441, 393 and 15675 for the HA , VV , $t\bar{t}$ and V +jets production processes, respectively, in our simulation assuming the integrated luminosity of 100 fb^{-1} . Notice that at the pre-selection, the charges of the muons and the tau-jets are not required to be opposite in each to collect all the $2\mu 2\tau_h$ signals through the 4τ decay of the Higgs boson pairs. Instead, we require the charge sum of the four leptons to vanish. The number of signal events are about two orders of the magnitude smaller than background contributions.

In the left panel in FIG. 1, we show distributions of the invariant mass $M_{\mu\mu}$ of a muon pair in the $2\mu 2\tau_h$ channel after the pre-selection. The solid black line is for the signal HA production, the dashed red line is for the VV production, the dotted green line is for the $t\bar{t}$ production and the dot-dashed blue line is for the V +jets production. Numbers of events for each process are normalized so as to correspond to the integrated luminosity of 100 fb^{-1} . The invariant mass distribution of the dimuon for the HA production shows two sharp peaks at $M_{\mu\mu} \simeq 130$ GeV and 170 GeV which corresponds to a pair of primary muons from the decay of extra neutral Higgs bosons. Due to the secondary muon from the decay of tau leptons, the signal events behave a broad distribution peaked around 50 GeV as well. The dimuon invariant mass distributions for the VV and V +jets processes have a peak at $M_{\mu\mu} \simeq m_Z$ through the decay of the Z boson into the dimuon. The numbers of events in the distributions for the VV and V +jets processes decrease rapidly at high mass regions, but that for the $t\bar{t}$ process decreases only slowly.

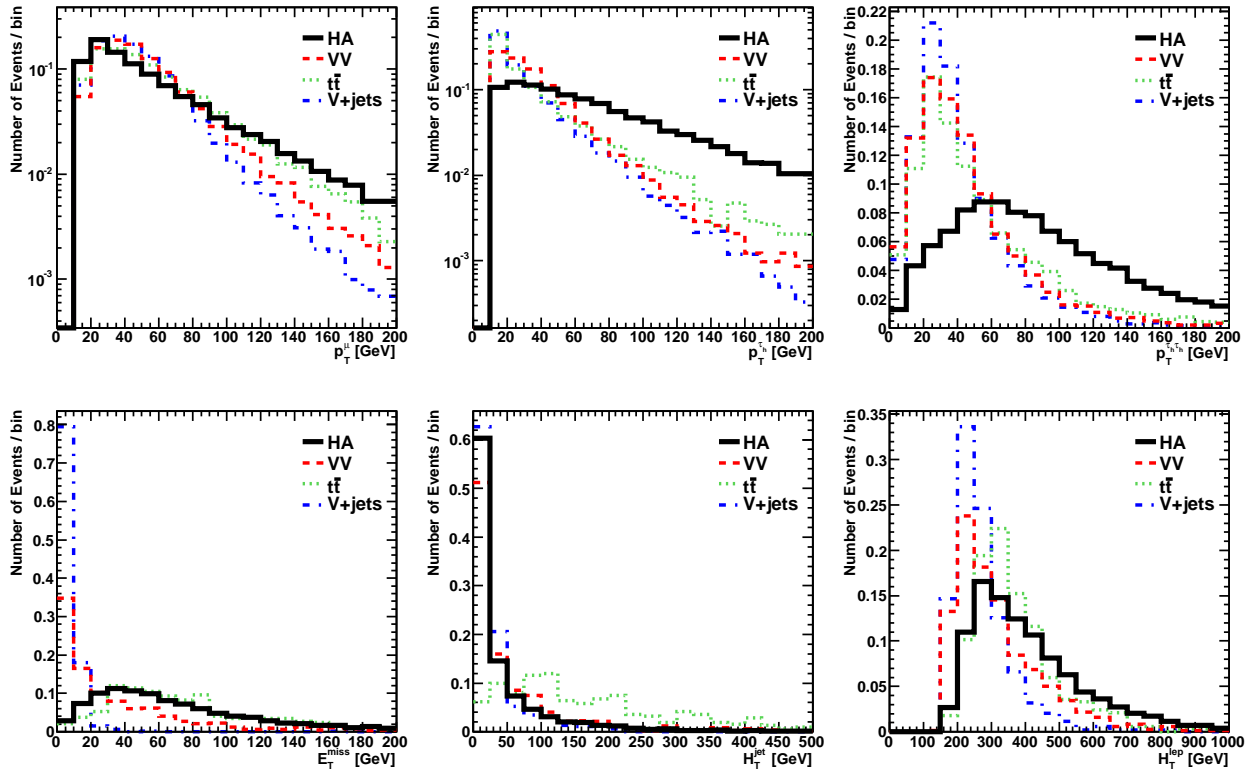


FIG. 2: Distributions of kinematical variables for the $2\mu 2\tau_h$ channel. Line descriptions follow those in FIG. 1.

$2\mu 2\tau_h$ event analysis	HA	$\phi^0 H^\pm$	VV	$t\bar{t}$	V+jets	s/b	S (100 fb $^{-1}$)
Pre-selection	91.0	7.7	441.	393.	15675.	10^{-2}	0.8
$p_T^{\tau_h} > 40$ GeV	41.1	1.7	37.7	33.4	548.	0.1	1.7
$\cancel{E}_T > 30$ GeV	33.1	1.6	14.7	29.9	5.1	0.7	4.5
$H_T^{\text{jet}} < 50$ GeV	24.0	1.2	9.7	4.3	3.1	1.4	5.1
$H_T^{\text{lep}} > 250$ GeV	21.6	1.1	8.6	3.7	1.0	1.7	5.1
$(m_Z)_{\mu\mu} \pm 10$ GeV	18.8	1.0	2.1	3.3	1.0	3.1	5.8
O.S. muons	13.2	0.6	2.0	3.3	1.0	2.2	4.4
$0 \leq z_{1,2} \leq 1.1$	2.9	0.1	1.0	0.6	0.	1.9	1.9
$(m_Z)_{\tau\tau} \pm 20$ GeV	2.7	0.1	0.2	0.6	0.	3.5	2.3

TABLE III: Table for background reductions in the $2\mu 2\tau_h$ channel. Listed are the expected number of events for the integrated luminosity of 100 fb $^{-1}$ at the LHC $\sqrt{s} = 14$ TeV. “O.S.” stands for “opposite-sign”.

In FIG. 2, we show the distributions of the transverse momentum p_T^μ for a muon, that p_T^h for a tau-jet, that $p_T^{\tau_h\tau_h}$ for a tau-jet pair, the missing transverse energy $\cancel{E}_T (= |\vec{p}_T^{\text{miss}}|)$, the hadronic and leptonic scalar sum of the transverse momentum $H_T^{\text{jet}} (= \sum_{\text{jet}} |p_T|)$ and $H_T^{\text{lep}} (= \sum_{\ell, \tau_h} |p_T|)$, respectively, in the $2\mu 2\tau_h$ channel after the pre-selection. In all panels in FIG. 2, numbers of the signal and background events are normalized to be unity. Line descriptions follow those in FIG. 1.

Taking into account the difference of distributions between signal and background events in FIG. 2, we employ the following selection cuts;

$$p_T^{\tau_h} > 40 \text{ GeV}, \quad (7a)$$

$$\cancel{E}_T > 30 \text{ GeV}, \quad (7b)$$

$$H_T^{\text{jet}} < 50 \text{ GeV}, \quad (7c)$$

$$H_T^{\text{lep}} > 250 \text{ GeV}, \quad (7d)$$

$$|M_{\mu\mu} - m_Z| > 10 \text{ GeV}. \quad (7e)$$

Here, we briefly explain the background reduction strategy with these cuts. The transverse momentum of tau-jets in signal events is relatively larger than that in the background processes due to the heavier mass of Higgs bosons than those of Z and W bosons. Therefore a relatively high p_T cut for tau-jets could enhance the signal-to-background ratio. We note that the high p_T requirement of tau-jets is also suitable for the stable tau-tagging efficiency at hadron colliders [44]. Background events from the V +jets process contain two mis-identified tau-jets from the ISR jets, with a muon pair which comes from the $Z/\gamma^* \rightarrow \mu^+\mu^-$ decay. Therefore, V +jets background events tend to have small \cancel{E}_T , and the cut on \cancel{E}_T is expected to reduce the V +jets background significantly. The background contribution from the $t\bar{t}$ events can be reduced by using the cut on H_T^{jet} , because the $t\bar{t}$ events tend to contain many jets due to the b quark fragmentation and ISR/FSR, even though two of them are mis-identified as tau-jets. The cut on H_T^{lep} can reduce the VV and V +jets backgrounds significantly. Furthermore, the events which contain $Z \rightarrow \mu^+\mu^-$ can be reduced by rejecting the events with the invariant mass of the muon pair close to m_Z .

The results of the signal/background reduction are summarized at each step in TABLE III. We show the expected numbers of events for the integrated luminosity of $L = 100 \text{ fb}^{-1}$ for each process. In the table, we also include the signal events from the charged Higgs boson associated production process $pp \rightarrow \phi^0 H^\pm$. The signal-to-background ratio s/b is evaluated at each step of the cuts, where s and b represent the numbers of signal and background events, respectively, taking all the HA and $\phi^0 H^\pm$ production processes as the signal events. In order to evaluate the signal significance, we use the significance estimator S defined as [45]

$$S = \sqrt{2[(s+b)\ln(1+s/b) - s]}, \quad (8)$$

which is also given at each step of the selection cuts. The significance S is proportional to the square root of the integrated luminosity. We choose the selection cuts basically to enhance S . However, since our background events are estimated based on the leading order cross sections and distributions with limited statistics, the s/b ratio should not be small but preferably $\mathcal{O}(1)$ to make our results conservative. The largest significance can be obtained after the m_Z -window cut, where the number of the signal events is expected to be about 20 while that of background events is about 6 giving $s/b \sim 3$ and $S \sim 6$ for $L = 100 \text{ fb}^{-1}$.

In the right panel in FIG. 1, we show the dimuon invariant mass distributions after the selection cuts (7a), (7b), (7c) and (7d). After these cuts, the signal process dominates the total events in the $2\mu 2\tau_h$ channel. Thus the two resonant peaks are more enhanced. The mass resolution is expected

to be quite well due to the fine resolution of the muon momentum measurement. On the other hand, the expected number of events for $L = 100 \text{ fb}^{-1}$ is not sufficient to observe the peaks in the $M_{\mu\mu}$ distribution.

Now let us consider the detail of the events for the signal process from HA production. As we have mentioned, the $2\mu 2\tau_h$ final state arises through the $HA \rightarrow 4\tau$ and $HA \rightarrow 2\mu 2\tau$ decays of the Higgs bosons. Assuming the dominant branching ratio of $\mathcal{B}(\phi^0 \rightarrow \tau^+\tau^-) \simeq 1$, the probability to get to the $2\mu 2\tau_h$ final state from the former route is expressed as $\binom{4}{2} [\mathcal{B}(\tau \rightarrow \mu)]^2 [\mathcal{B}(\tau \rightarrow \tau_h)]^2$, where the binomial coefficient $\binom{4}{2} = 6$. On the other hand, the probability through the latter route is $2\mathcal{B}(\phi^0 \rightarrow \mu^+\mu^-) [\mathcal{B}(\tau \rightarrow \tau_h)]^2$. Thus, the ratio of the probabilities through the two routes is $3 [\mathcal{B}(\tau \rightarrow \mu)]^2 / \mathcal{B}(\phi^0 \rightarrow \mu^+\mu^-)$, which is predicted to be about 26 in the Type-X THDM. However, in the actual events, the ratio of the expected numbers of the events through the two routes suffers from the acceptance cuts on the muons. Especially, the p_T cut on the muons is expected to reduce the ratio, since the muons from the decay of tau leptons have relatively small transverse momentum. From the left panel in FIG. 1, the ratio of the number of the excess events at the sharp $M_{\mu\mu}$ peaks to the number of the events in the continuous distribution is found to be $6.6/84.4 \sim 1./12.8$. After the selection cuts up to the cut on H_T^{lep} in (7d), the ratio becomes $1.6/20 \sim 1./12.5$ (see the right panel in FIG. 1). Thus, we find our selection cuts do not significantly modify the ratio. With this fact, the branching ratios of $\mathcal{B}(\phi^0 \rightarrow \mu^+\mu^-)$ can be measured as

$$\mathcal{B}(\phi^0 \rightarrow \mu^+\mu^-) = \frac{\text{Number of the excess events at } M_{\mu\mu} \text{ peaks}}{\text{Number of events in the continuous dist.}} \times 3 [\mathcal{B}(\tau \rightarrow \mu)]^2 \times \epsilon, \quad (9)$$

where ϵ is the correction factor which reflects the difference of the kinematical distributions of the muons between the 4τ and $2\mu 2\tau$ decays of Higgs bosons resulting the difference of the kinematical acceptance of the muons. It could be simulated by using the kinematical distributions of the muons calculated theoretically and the acceptance cuts for muons. In our simulation, we get $\epsilon \sim 0.5$, thus the ratio of the muon acceptance in the 4τ decay to that in the $2\tau 2\mu$ decay is $\sqrt{0.5} \sim 0.7$.

Once the peaks in the $M_{\mu\mu}$ distribution are observed with the sufficient number of events, the measurement of the branching ratio into the dimuon is possible. If we consider the case where the Higgs bosons decay into the other modes as well, such like weak bosons or quarks, the left-hand side of Eq. (9) is replaced by the ratio of the branching ratios or the partial decay widths for muons and tau leptons, which is exactly the ratio of the square of the Yukawa couplings to muons and tau leptons.

Next, we turn our interest to the tau-jet observables. One of the attractive features of the $2\mu 2\tau_h$ channel is that the four momenta of tau leptons are reconstructable, if the muon pair comes from the direct decay of one of the neutral Higgs bosons. In such a case, the missing momentum in the event is expected to come from the hadronic decay of tau leptons, and then the full kinematics of tau leptons can be reconstructed by using the collinear approximation for the relation of the momenta of the tau leptons and the tau-jets. To enhance the signal events where one of the Higgs bosons decays directly into the dimuon, we require the muon pair to have opposite-sign charges. Then, we apply the collinear approximation for the tau-jets to determine the four momenta of the tau leptons.

Here, we briefly explain the collinear approximation to calculate the four momenta of the tau leptons. If tau leptons are energetic, the missing momentum from its decay would be along the direction of the charged track (either a charged hadron (hadrons) or a charged lepton), $\vec{p}^{miss} \simeq c\vec{p}^{\tau_j}$, where \vec{p}^{miss} , \vec{p}^{τ_j} are the momenta of the neutrino and the charged track, respectively. The proportionality constant c can be determined by fixing \vec{p}^{miss} . Accordingly, the momentum of the decaying tau lepton can be approximately reconstructed as $\vec{p}^\tau \simeq (1+c)\vec{p}^{\tau_j} \equiv z^{-1}\vec{p}^{\tau_j}$, where z is the momentum fraction of the charged track from the parent tau lepton. At hadron colliders, the transverse components of the missing momentum \vec{p}_T can be measured. Assuming that the missing transverse momentum of the event is accounted solely by the missing particles in the decays of tau leptons, and applying the collinear approximation for both the tau leptons, the missing transverse momentum can be expressed by the momenta of charged tracks, as $\vec{p}_T \simeq \vec{p}_T^{miss1} + \vec{p}_T^{miss2} \simeq c_1\vec{p}_T^{\tau_{j1}} + c_2\vec{p}_T^{\tau_{j2}}$. Unknown parameters c_1 and c_2 are determined by solving simultaneous equations. Using the resulting values of z_1 and z_2 , the invariant mass of the tau leptons pair is related with that of the tau-jets pair as $M_{\tau_h\tau_h}^2 \simeq z_1z_2M_{\tau\tau}^2$. The fractions z_1 and z_2 should be between 0 and 1. In our analysis, we set a 10% margin for the upper bound on the cut of the momentum fractions, i.e., $0 < z_{1,2} < 1.1$. This is to take into account the resolution of the momentum measurements and also the limitation of the validity of the collinear approximation. Actually, by taking the 10% margin the number of the signal events which have the solution is enhanced by about 10%, although s/b and S are almost unchanged. The lower limit of z is not significant because of the high p_T cut on the tau-jets.

In the left panel in FIG. 3, we show the $M_{\tau_h\tau_h}$ distributions, after requiring opposite-sign for the muon pair in TABLE III. In the right panel in FIG. 3, the $M_{\tau\tau}$ distributions of the pair of the reconstructed tau leptons from the two tau-jets are shown, while the events without the solution of the equations in the $0 < z_{1,2} < 1.1$ ranges are rejected. Similarly to the $M_{\mu\mu}$ distribution, two resonant peaks can be observed with relatively wide widths at the masses of the neutral Higgs bosons. Only a few backgrounds from VV and $t\bar{t}$ production are expected. The VV background can be further reduced by the cut on the m_Z -window for the reconstructed $M_{\tau\tau}$.

In the upper panels of FIG. 4, the double invariant mass distribution of $M_{\tau_h\tau_h}$ vs. $M_{\mu\mu}$ (left) and $M_{\tau\tau}$ vs. $M_{\mu\mu}$ (right) for the signal events are shown. In the distribution in the top-left panel, we can see two bands along the x -axis at $M_{\mu\mu} \simeq 130$ GeV and 170 GeV. In the distribution in the top-right panel, two peaks can be found around $(M_{\tau\tau}, M_{\mu\mu}) = (130, 170)$ and $(170, 130)$ [GeV]. In the lower panels we show the distributions of the sum of the background processes for the reference. The background events after solving the tau lepton momenta mostly have $M_{\tau\tau} \simeq m_Z$. Thus by the m_Z -window cut on $M_{\tau\tau}$, more rejections of the background are expected. This two dimensional invariant mass distribution gives an evidence for the pair production of neutral Higgs bosons which dominantly decay into the pair of tau leptons and occasionally into the pair of muons directly. Accurate mass measurement is also possible, when we have sufficient statistics.

Similar analysis to the $2\mu 2\tau_h$ channel can be performed for the other four-lepton channels with two or more muons, which are $2\mu 1\tau_h 1e$, $3\mu 1\tau_h$, 4μ , $3\mu 1e$ and $2\mu 2e$ channels. In the channels where there are three or more muons, combinatorial complexity may be avoided by choosing the pair of

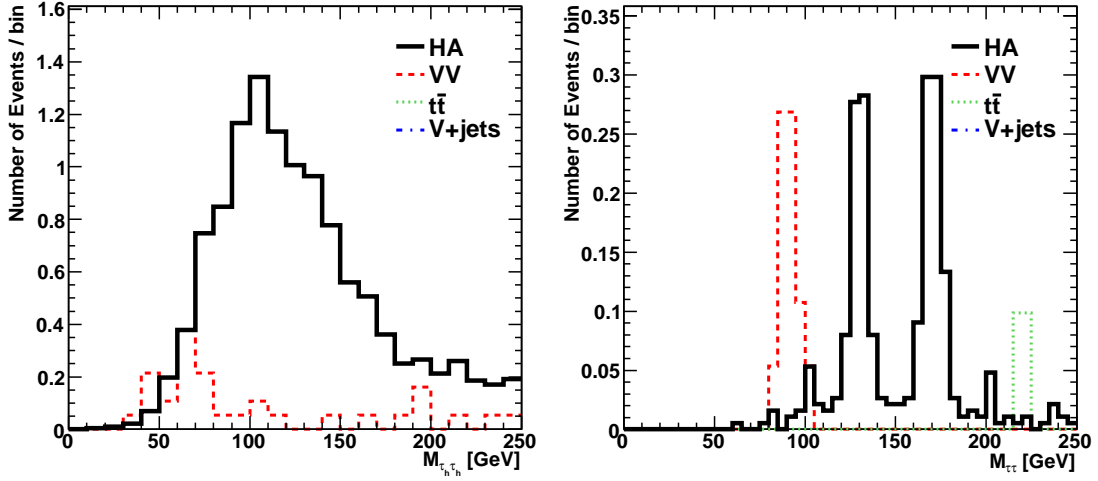


FIG. 3: Invariant mass distributions of the tau-jet pair $M_{\tau_h\tau_h}$ (left) after the selection cuts up to the opposite-charge muon pair in TABLE III, and those of the tau-lepton pair reconstructed by using the collinear approximation $M_{\tau\tau}$ (right) in the $2\mu 2\tau_h$ channel. Only the events with a solution of the collinear approximation in $0 < z_{1,2} < 1.1$ ranges are used for the latter distribution. Signal events plotted in the solid black line are generated with $m_H = 130$ GeV and $m_A = 170$ GeV. Contributions from the VV background are also shown in the dashed red line.

Lepton channels	$2\mu 2\tau_h$		$2\mu 1\tau_h 1e$		$3\mu 1\tau_h$		4μ		$3\mu 1e$		$2\mu 2e$	
	s/b	(S)	s/b	(S)	s/b	(S)	s/b	(S)	s/b	(S)	s/b	(S)
Pre-selection	98.7/16507.	(0.8)	35.7/154.	(2.8)	14.3/162.	(1.1)	0.9/401.	(0.0)	2.6/8.9	(0.8)	3.3/647.	(0.1)
$p_T^{\tau_h} > 40$ GeV	42.8/618.	(1.7)	23.6/46.2	(3.2)	9.4/46.8	(1.3)	-	(-)	-	(-)	-	(-)
$\cancel{E}_T > 30$ GeV	34.7/ 59.7	(4.5)	19.2/25.3	(3.3)	7.7/27.5	(1.4)	0.7/4.2	(0.3)	2.0/5.8	(0.8)	2.5/5.7	(1.0)
$H_T^{\text{jet}} < 50$ GeV	25.2/17.1	(5.1)	-	(-)	-	(-)	-	(-)	-	(-)	-	(-)
$H_T^{\text{lep}} > 250$ GeV	22.7/13.3	(5.1)	15.7/18.4	(3.3)	6.5/20.2	(1.4)	0.6/2.1	(0.4)	1.5/2.8	(0.8)	1.7/3.0	(0.9)
$(m_Z)_{\mu\mu} \pm 10$ GeV	19.8/6.4	(5.8)	13.7/2.3	(5.9)	5.4/5.1	(2.1)	0.5/0.5	(0.6)	1.3/0.6	(1.3)	1.3/0.3	(1.6)
O.S. muons	13.8/6.3	(4.4)	9.5/2.0	(4.6)	-	(-)	-	(-)	-	(-)	0.9/0.3	(1.3)
$0 \leq z_{1,2} \leq 1.1$	3.0/1.6	(1.9)	3.0/1.0	(2.3)	2.0/1.3	(1.5)	0.4/0.2	(0.7)	0.7/0.3	(1.0)	0.4/0.2	(0.8)
$(m_Z)_{\tau\tau} \pm 20$ GeV	2.8/0.8	(2.3)	2.8/0.3	(3.0)	1.8/0.7	(1.7)	0.3/0.1	(0.8)	0.6/0.2	(1.0)	0.4/0.0	(-)

TABLE IV: Summary of event rejections for the four-lepton channels with two or more muons. The signal-to-background ratio s/b and the significance S for $L = 100 \text{ fb}^{-1}$ are listed. The cut on H_T^{jet} is not imposed for the channels with one or less tau-jet. A pairing rule of dimuons for the channels with three or more muons is explained in the text. In the $2\mu 2e$ channel, an additional cut of $|M_{ee} - m_Z| > 10$ GeV is applied at the cut of $(m_Z)_{\mu\mu} \pm 10$ GeV.

opposite-sign muons which gives the largest transverse momentum of the muon pair. The signal-to-background ratio and the expected significance for these channels by applying the selection cuts similar to those for the $2\mu 2\tau_h$ channel are summarized in TABLE IV for $L = 100 \text{ fb}^{-1}$. The cut variables are not optimized for each channel. The cut on H_T^{jet} is not imposed for the channels with one or less tau-jet, since for these channels $t\bar{t}$ process are negligible from the pre-selection level.

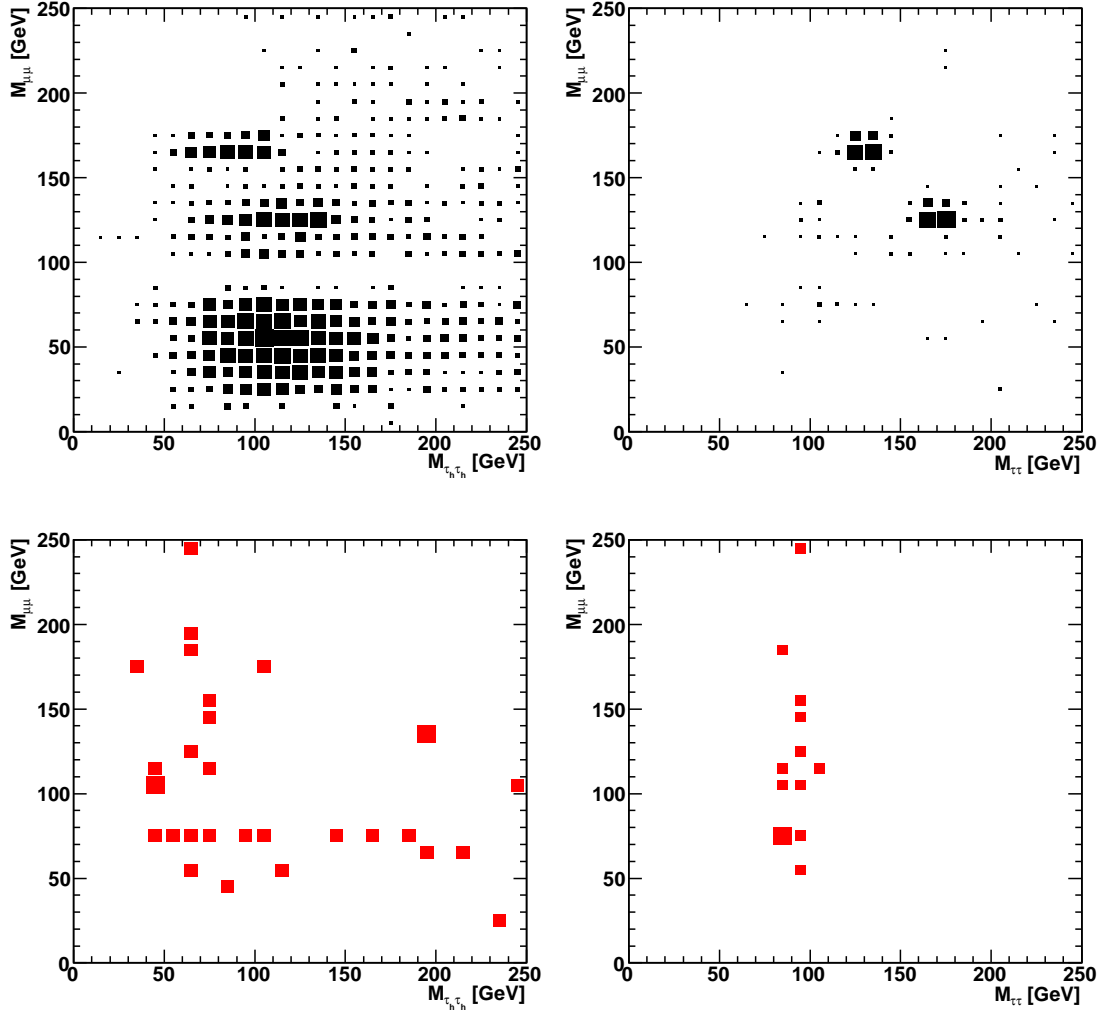


FIG. 4: Two dimensional plots for the invariant mass distributions $M_{\mu\mu}$ vs. $M_{\tau_h\tau_h}$ (upper-left) and $M_{\mu\mu}$ vs. $M_{\tau\tau}$ (upper-right) in the signal processes $pp \rightarrow HA$, where $m_H = 130$ GeV and $m_A = 170$ GeV are taken. The distributions for the background events are also given in the lower panels. The normalization of the box-plot in each panel is set separately.

The collinear approximation is applied for the two leptons other than the two opposite-sign muons. The large s/b and S can be observed for the $2\mu 1\tau_h 1e$ channel as well, where the $t\bar{t}$ background is less significant than for the $2\mu 2\tau_h$ channel.

By the requirement of opposite-sign charges in the dimuon, the background processes hardly lose events, while the signal process reduces one third of events which is consistent with a naive expectation by counting combinatory. It means, in the other word, that the requirement of same-sign charges in the dimuon extracts the signal events with only small background contribution mainly from the VV process. This is also useful to find the evidence on top of the SM process in the various channels with two muons or also two electrons. Those channels also appear in the latter.

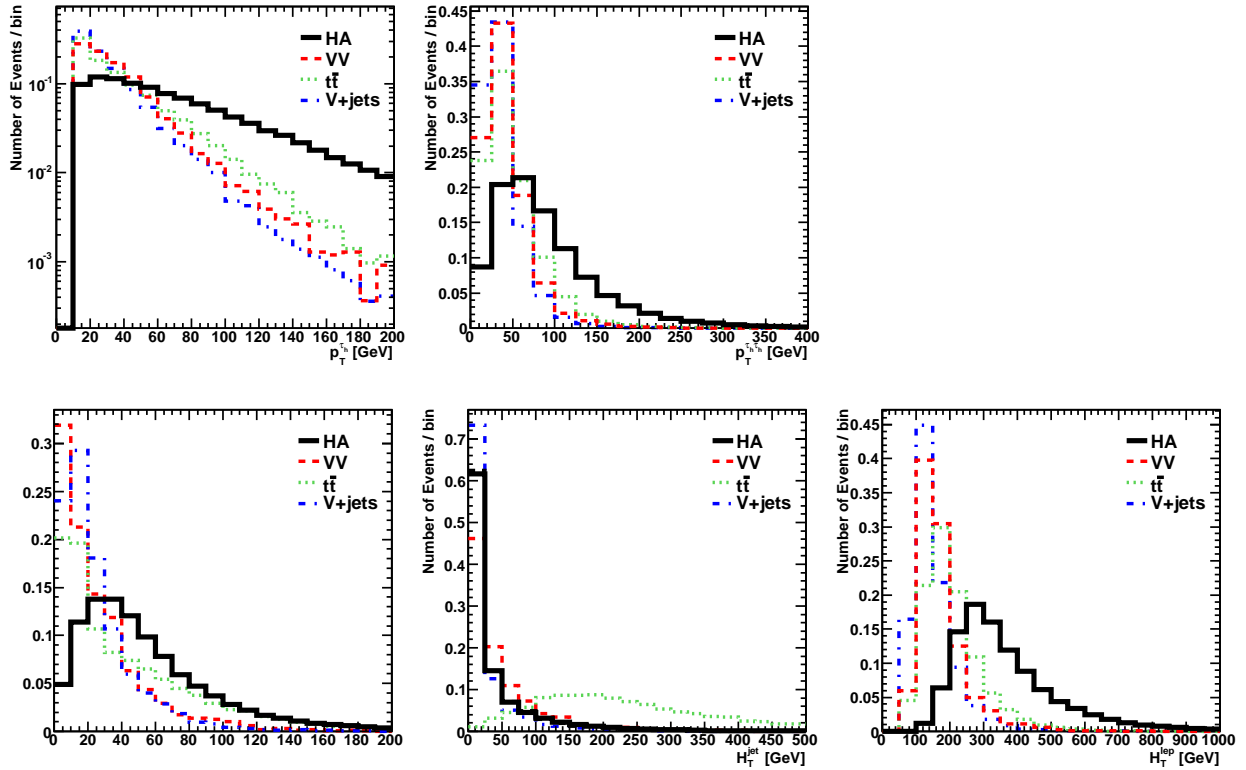


FIG. 5: Distributions of kinematical variables for the $4\tau_h$ channel. Line descriptions follow those in FIG. 1.

2. Four-lepton channels with two or more tau-jets

Due to the dominant branching ratio into tau leptons, a large number of events is expected in the channels with high tau-jet multiplicity, thus an excess beyond the SM expectation may be detectable in these channels. On the other hand, four-lepton channels without a primary muon pair from the decays of neutral Higgs bosons are hard to be kinematically reconstructed.

First, we consider the $4\tau_h$ channel. Since this channel contains only hadronic objects but no leptonic objects in an event, the triggering efficiency may not be as good as those in the channels with muons. However, the requirement of the high- p_T tau-jet shall stabilize the abstraction of the events in this channel, and we expect at least relative information would be available such as kinematical distributions and the signal-to-background ratio. Then, we present results and comments for the other four-lepton channels with two or more tau-jets. In the end of this subsection, we also comment on the remaining four-lepton channels.

After the pre-selection with the requirement of the vanishing charge sum of the four hadronic tau-jets, the expected numbers of events are 324, 147, 797 and 5105 for HA , VV , $t\bar{t}$ and V +jets production processes, respectively, for $L = 100 \text{ fb}^{-1}$. The dominant background contributions come from Z +jets production followed by the $Z \rightarrow \tau^+\tau^-$ decay and the hadronic decays of the tau leptons with two more tau-jets which are mis-identified from the ISR jets.

$4\tau_h$ event analysis	HA	$\phi^0 H^\pm$	VV	$t\bar{t}$	$V+\text{jets}$	s/b	S (100 fb $^{-1}$)
Pre-selection	324.	52.8	147.	797.	5105.	0.1	4.7
$p_T^{\tau_h} > 40$ GeV	67.2	4.9	2.0	14.7	21.7	1.9	9.4
$\cancel{E}_T > 30$ GeV	48.6	4.4	1.1	7.6	10.4	2.8	9.3
$H_T^{\text{jet}} < 50$ GeV	34.2	3.4	0.5	0.8	8.2	3.9	8.7
$H_T^{\text{lep}} > 350$ GeV	27.6	2.7	0.4	0.5	3.1	7.5	9.3

TABLE V: Table for the background reductions in the $4\tau_h$ channel.

In FIG. 5, we show distributions of the transverse momentum $p_T^{\tau_h}$ of the tau-jet, that $p_T^{\tau_h\tau_h}$ for the tau-jet pair, the missing transverse energy \cancel{E}_T and the scalar sum of the hadronic and leptonic transverse momentum, H_T^{jet} and H_T^{lep} , respectively. Distributions for all the signal and background processes are normalized to be unity. Line descriptions follow those in FIG. 1. In order to reject backgrounds, the following selection cuts are applied;

$$p_T^{\tau_h} > 40 \text{ GeV}, \quad (10a)$$

$$\cancel{E}_T > 30 \text{ GeV}, \quad (10b)$$

$$H_T^{\text{jet}} < 50 \text{ GeV}, \quad (10c)$$

$$H_T^{\text{lep}} > 350 \text{ GeV}. \quad (10d)$$

Reductions of the signal and background events are summarized at each cut in TABLE V. For $L = 100 \text{ fb}^{-1}$, an expected significance S is about 5 at the pre-selection level, and reaches to around 9 after the selection cuts. The signal-to-background ratio s/b rises to about 8 at the end of all the selection cuts. Thus, finding the evidence in this channel seems very promising. It may be even possible at more earlier stage at the LHC. The more tight cut for the p_T of the tau-jets can enhance the signal-to-background ratio, while slightly reduces the significance. We note that we have not estimated the background contributions from pure QCD processes as well as the $V+\text{jet}$ production process followed by hadronic decays of weak gauge bosons, which could survive after the selection cuts if all the four tau-jets are mis-identified. We expect that a severe \cancel{E}_T cut should sufficiently reduce the number of events for these processes.

Since in the $4\tau_h$ events all the four hadronic decays of tau leptons could yield missing momenta, the collinear approximation analysis used in the $2\mu 2\tau_h$ channel cannot be applied, and the masses of the Higgs bosons cannot be reconstructed kinematically. However, as we will see below, distributions of the invariant mass of the tau-jet pair are useful to obtain the information of the mass of the Higgs bosons. To resolve combinatorial complexity from the four tau-jets, one invariant mass is constructed from the tau-jet pair with opposite-charges which gives the largest $p_T^{\tau_h\tau_h}$, and the other is constructed from the remaining tau-jet pair. Then, the invariant masses of the two tau-jet pairs, $M_{\tau_h\tau_h}$ and $m_{\tau_h\tau_h}$, are defined by $M_{\tau_h\tau_h} \geq m_{\tau_h\tau_h}$.

In FIG. 6, distributions of $M_{\tau_h\tau_h}$ (left) and $m_{\tau_h\tau_h}$ (right) are shown for the signal events from HA production, while the background contributions are omitted because they are negligible. In the

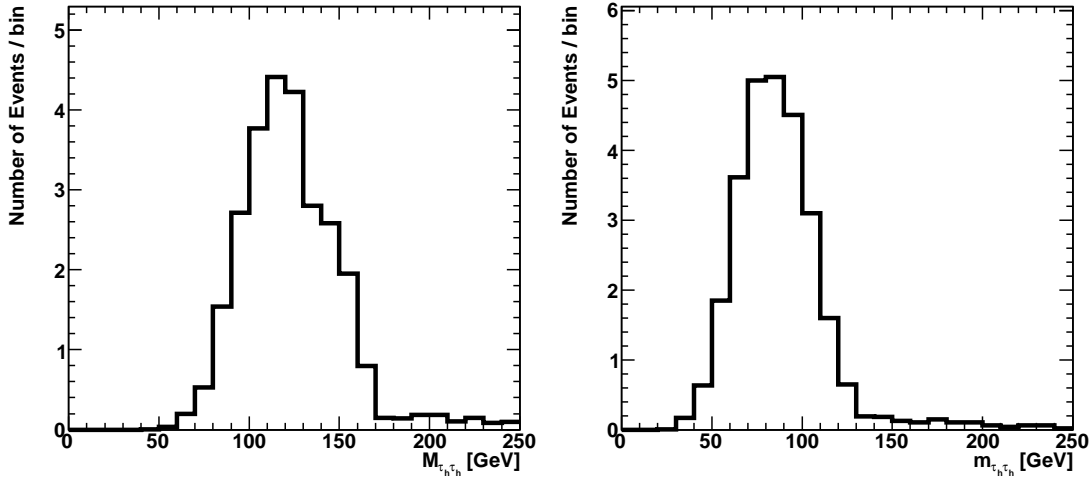


FIG. 6: Distributions of the invariant mass of the opposite-charge tau-jet pair, $M_{\tau_h\tau_h}$ (left) and $m_{\tau_h\tau_h}$ (right), where $M_{\tau_h\tau_h} \geq m_{\tau_h\tau_h}$ in the $4\tau_h$ channel. Signal events are generated with $m_H = 130$ GeV and $m_A = 170$ GeV.

$M_{\tau_h\tau_h}$ distribution in the left panel, we can see an endpoint of the distribution at $M_{\tau_h\tau_h} \simeq 170$ GeV which corresponds to $m_A = 170$ GeV. Another mass information for $m_H = 130$ GeV can be seen as an endpoint in the $m_{\tau_h\tau_h}$ distribution in the right panel or may be found as a bump in the $M_{\tau_h\tau_h}$ distribution. Thus, if sufficient numbers of events are obtained by accumulating the integrated luminosity such like a few thousand fb^{-1} at the LHC, it should be possible to extract the mass of the Higgs bosons by these distributions. In FIG. 7, we also present the two dimensional distribution of the invariant masses $M_{\tau_h\tau_h}$ and $m_{\tau_h\tau_h}$ for the signal events in the $4\tau_h$ channel after the selection cuts.

Similar analysis to the $4\tau_h$ channel can be performed for the other four-lepton channels with two or more hadronic tau-jets; such as $3\tau_h1\mu$, $3\tau_h1e$, $2\tau_h1\mu1e$ and $2\tau_h2e$ channels. Due to the expected large number of events, many of them can give large S with large s/b by the similar selection cuts for $L = 100 \text{ fb}^{-1}$. Measurements of these channels would provide a test of the signatures of tau leptons in the extensive channels, and thus they are useful to probe the production of the tau-lepton-specific Higgs bosons. The endpoint study such like in FIG. 6 may not be suitable for the invariant mass distributions including μ or e , because the momentum fraction z for the leptonic decays of tau leptons distributes mainly in a small z region [15]. The rest of the four-lepton channels are $1\tau_h1\mu2e$, $1\tau_h3e$, $1\mu3e$ and $4e$. However, except the $1\tau_h1\mu2e$ channel, the expected numbers of events are too small; a few events or less for $L = 100 \text{ fb}^{-1}$. The signal-to-background ratio and the estimated significance by applying the selection cuts for these channels are summarized in TABLE VI and VII assuming the integrated luminosity of 100 fb^{-1} .

Before closing the subsection for the four-lepton channels, we point out an interesting comparison between the $2\mu2\tau_h$ and $2\tau_h2e$ channels. Theoretically, the difference of the two channels

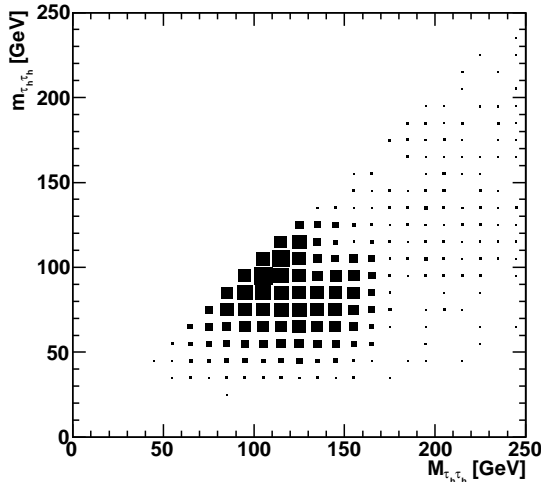


FIG. 7: Two dimensional distributions of the two opposite-sign tau-jet pair (M_{τ_h, τ_h} vs m_{τ_h, τ_h}) in the $4\tau_h$ channel after the selection cuts for the signal processes $pp \rightarrow HA$ with $m_H = 130$ GeV and $m_A = 170$ GeV.

arises from the direct decay of Higgs bosons into dimuons through the Yukawa couplings of Higgs bosons to muons. On the other hand, those to electrons are negligible, since $m_e^2/m_\mu^2 \simeq 2.3 \cdot 10^{-5}$. The invariant mass distribution of the dielectron in the $2\tau_h 2e$ channels is nothing but that of the dimuon in the $2\tau_h 2\mu$ channel except the absence of the two resonant peaks seen at $M_{\mu\mu} \simeq m_H$ and $M_{\mu\mu} \simeq m_A$. The common part of the distributions between the $2\mu 2\tau_h$ and $2\tau_h 2e$ channels should be originated from the 4τ decay, while the excess in the $2\mu 2\tau_h$ channel relative to the $2\tau_h 2e$ channel should be originated from the decay of the Higgs bosons directly into muons.

Experimentally, the efficiencies of finding electrons and muons are different due to the different isolation condition and acceptance cuts. In our simulation study, the normalization of the events could be corrected by naively multiplying for the number of events in the $2\tau_h 2e$ channel by 1.1, which is about the ratio of the finding efficiency for muons to that for electrons obtained by comparing the numbers of events in the $3\tau_h 1\mu$ and $3\tau_h 1e$ channels.

C. Charged Higgs boson associated production

At the hadron collider, charged Higgs bosons can be produced in association with the neutral Higgs bosons via the $pp \rightarrow W^{\pm*} \rightarrow \phi^0 H^\pm$ processes [22]. In the Type-X THDM, more than 99% of charged Higgs bosons decays into a tau lepton and a neutrino, and $0.35\% \simeq m_\mu^2/m_\tau^2$ does into a muon and a neutrino for $\tan\beta \gtrsim 2$ [9]. Therefore, the characteristic signatures for this process would be the three-lepton channels including many tau leptons or muons accompanied with large missing momentum.

There are ten kinds of the three-lepton channels. Following the analysis of the four-lepton channels, we first present an analysis for the three-lepton channels with two or more muons, then we present analysis for those with two or more tau-jets. Brief summary of the analysis for the rest

Lepton channels	$4\tau_h$	$3\tau_h1\mu$	$3\tau_h1e$	$2\tau_h1\mu1e$	$2\tau_h2e$
	s/b (S)	s/b (S)	s/b (S)	s/b (S)	s/b (S)
Pre-selection	377./6050. (4.8)	302./4208. (4.6)	278./3883. (4.4)	166./917. (5.3)	74.4/13202. (0.6)
$p_T^{\tau_h} > 40$ GeV	72.1/38.5 (9.5)	87.2/70.2 (8.9)	80.2/72.2 (8.2)	71.7/67.5 (7.6)	32.4/479. (1.5)
$\cancel{E}_T > 30$ GeV	53.0/19.0 (9.3)	69.3/54.6 (8.0)	63.4/53.8 (7.5)	58.0/58.6 (6.7)	26.3/38.6 (3.8)
$H_T^{\text{jet}} < 50$ GeV	37.6/9.6 (8.7)	49.0/17.4 (8.9)	44.9/23.0 (7.6)	41.7/13.7 (8.5)	18.7/16.0 (4.0)
$H_T^{\text{lep}} > 350$ GeV	30.3/4.0 (9.3)	34.5/8.4 (8.4)	31.4/10.9 (7.2)	24.2/3.8 (8.0)	10.7/8.2 (3.2)
$(m_Z)_{ee} \pm 10$ GeV	- (-)	- (-)	- (-)	- (-)	9.3/2.5 (4.2)

TABLE VI: Summary of event rejections by the selection cuts for the four-lepton channels with two or more tau-jets.

Lepton channels	$1\tau_h1\mu2e$	$1\tau_h3e$	$1\mu3e$	$4e$
	s/b (S)	s/b (S)	s/b (S)	s/b (S)
Pre-selection	29.2/132. (2.5)	8.7/120. (0.8)	1.7/7.6 (0.6)	0.4/268. (0.0)
$p_T^{\tau_h} > 40$ GeV	19.3/38.6 (2.9)	5.6/34.2 (0.9)	- (-)	- (-)
$\cancel{E}_T > 30$ GeV	15.5/22.1 (3.0)	4.6/19.2 (1.0)	1.2/3.4 (0.6)	0.3/2.6 (0.2)
$(m_Z)_{ee} \pm 10$ GeV	13.6/2.4 (5.8)	4.0/6.5 (1.4)	1.1/1.2 (0.9)	0.2/0.7 (0.2)

TABLE VII: Summary of event rejections by the selection cuts for the rest of the four-lepton channels.

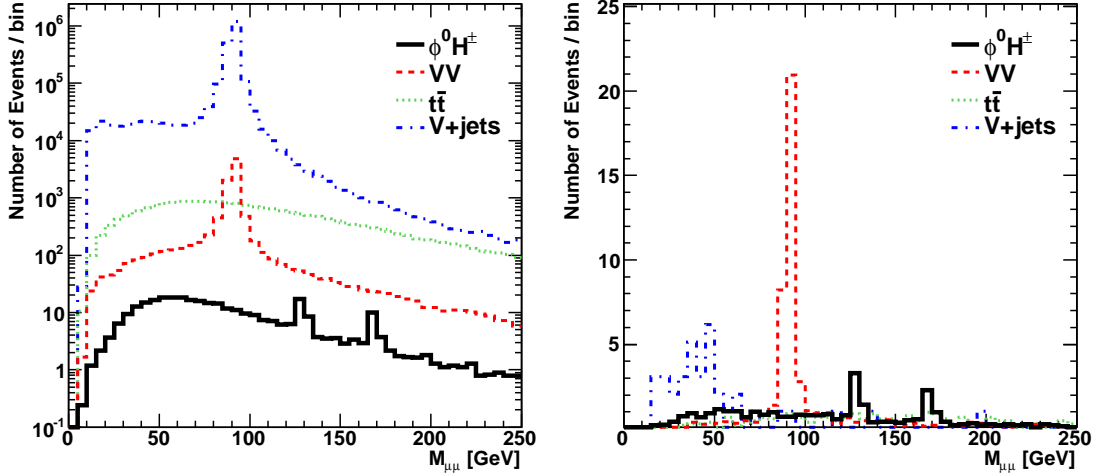


FIG. 8: The dimuon invariant mass distribution for the $2\mu1\tau_h$ channel after the pre-selection (left) and after the selection cuts before the cut on the m_Z -window in TABLE VIII (right). For the signal process, $m_H = 130$ GeV, $m_A = 170$ GeV and $m_{H^\pm} = 150$ GeV are taken.

of the three-lepton channels is presented after a while.

1. Three-lepton channels with two or more muons

In the $2\mu1\tau_h$ channel, the two muons can be originated from the decay of H or A , or one muon comes directly from H^\pm and the other comes secondarily through the leptonic decay of the tau

$2\mu 1\tau_h$ event analysis	HA	$\phi^0 H^\pm$	VV	$t\bar{t}$	$V+\text{jets}$	s/b	S (100 fb $^{-1}$)
Pre-selection	103.	341.	10380.	22683.	2297490.	10^{-4}	0.3
$p_T^{\tau_h} > 40$ GeV	71.4	230.	3147.	6690.	455178.	10^{-3}	0.4
$\cancel{E}_T > 80$ GeV	25.0	110.	244.	2659.	260.	10^{-2}	2.4
$H_T^{\text{jet}} < 30$ GeV	10.3	62.8	122.	96.5	102.	0.2	3.9
$H_T^{\text{lep}} > 350$ GeV	5.9	33.8	50.8	26.0	36.0	0.4	3.5
$(m_Z)_{\mu\mu} \pm 10$ GeV	5.4	30.8	17.4	23.0	34.0	0.5	3.9
O.S. muons	4.1	21.3	16.3	23.0	34.0	0.3	2.8
$p_T^{\mu\mu} > 80$ GeV	2.7	14.4	10.5	12.4	18.5	0.4	2.5
$(m_{\phi^0})_{\mu\mu} \pm 10$ GeV	0.7	5.4	1.9	2.7	1.0	1.1	2.3

TABLE VIII: Table for background reductions in the $2\mu 1\tau_h$ channel.

leptons. In the former case, the two muons must have opposite charges, and the distribution of their invariant mass shows resonance peaks at the mass of neutral Higgs bosons.

In the left panel in FIG. 8, we plot the invariant mass distribution of the muon pair for the $2\mu 1\tau_h$ channel after the pre-selection. The distributions are scaled to the expected number of the events for $L = 100 \text{ fb}^{-1}$ for each signal and background process. The expected number of events from the signal $\phi^0 H^\pm$ (and HA) process is four orders of magnitude smaller than that for the background processes, where the dominant contributions come from the Z +jets process.

To extract the signal events, we consider the selection cuts on this channel. In FIG. 9, we plot distributions of the transverse momentum p_T^μ for a muon, that $p_T^{\tau_h}$ for a tau-jet and that $p_T^{\tau_h\tau_h}$ for a tau-jet pair, the missing transverse energy \cancel{E}_T , and the scalar sum H_T^{jet} and H_T^{lep} of hadronic and leptonic transverse momentum, respectively, in the $2\mu 1\tau_h$ events after the pre-selection. Looking at the distributions in FIG. 9, we perform the following selection cuts to extract signal events in the $2\mu 1\tau_h$ channels;

$$p_T^{\tau_h} > 40 \text{ GeV}, \quad (11a)$$

$$\cancel{E}_T > 80 \text{ GeV}, \quad (11b)$$

$$H_T^{\text{jet}} < 30 \text{ GeV}, \quad (11c)$$

$$H_T^{\text{lep}} > 350 \text{ GeV}, \quad (11d)$$

$$|M_{\mu\mu} - m_Z| > 10 \text{ GeV}. \quad (11e)$$

Reductions of the number of events are summarized in each step in TABLE VIII. After the m_Z -window cut on the $M_{\mu\mu}$ distribution, the number of events for signal processes is ~ 36 , while the number of background events is expected to be ~ 74 . Although the s/b ratio is less than one, the significance S reaches to ~ 4 for $L = 100 \text{ fb}^{-1}$. Therefore, if a reliable background estimation is achieved, the excess of the observed events could be the signature for the production of the neutral and charged Higgs bosons.

In the right panel in FIG. 8, we plot the $M_{\mu\mu}$ distribution after the selection cuts up to the cut on H_T^{lep} . After the selection cuts, the $M_{\mu\mu}$ distribution in the V +jets background events tends to drop quickly before $M_{\mu\mu} \simeq 50 \text{ GeV}$. This is due to the requirement of the large \cancel{E}_T , thus the

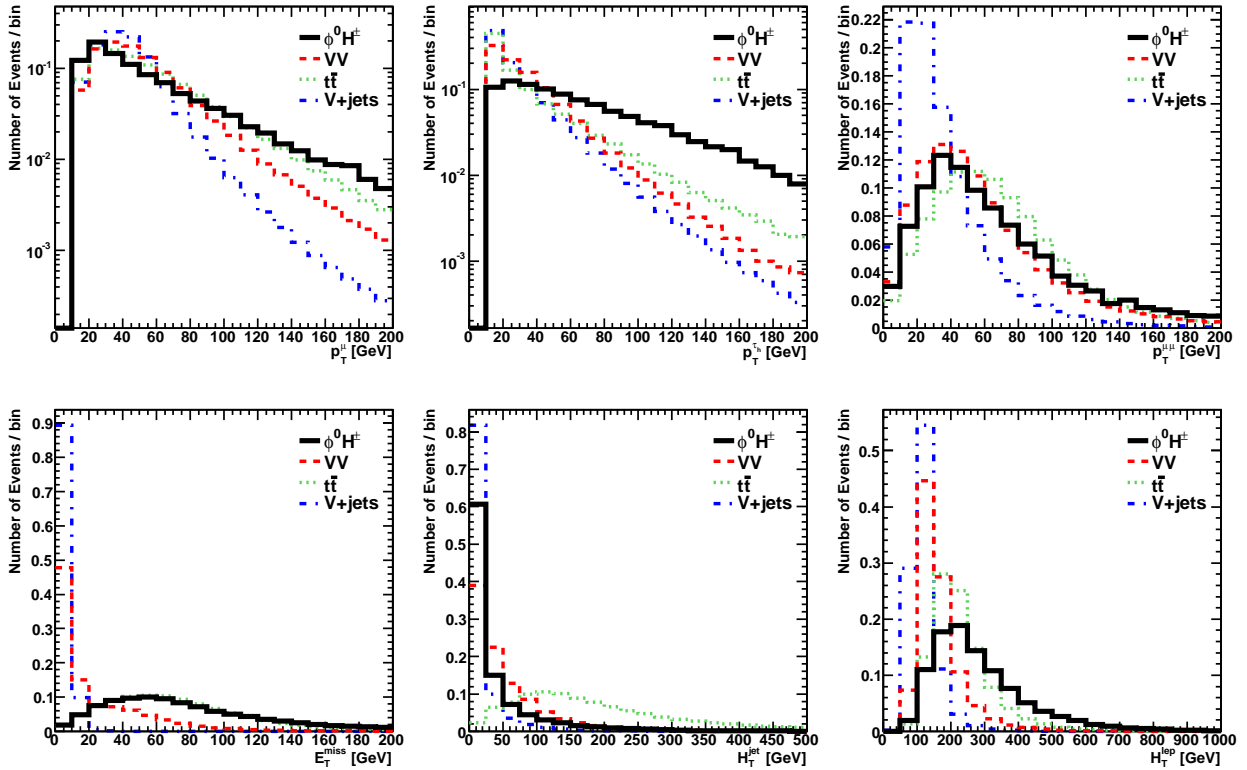


FIG. 9: Distributions of kinematical variables for the $2\mu 1\tau_h$ channel. Line descriptions follow those in FIG. 1.

events with a muon pair which directly comes from the decay of Z bosons are mostly rejected, but the events with a muon pair from the $Z \rightarrow \tau^+ \tau^-$ decay followed by the muonic decays of the tau leptons remain with one mis-identified tau-jet in the $2\mu 1\tau_h$ channel. The VV backgrounds mostly come from WZ production followed by $Z \rightarrow \mu^+ \mu^-$ and $W^\pm \rightarrow \tau^\pm \nu$ decays. Thus, the $M_{\mu\mu}$ distribution has a peak at $M_{\mu\mu} \simeq m_Z$, and the VV background events are reduced by the m_Z -window cut significantly. The signal events from $\phi^0 H^\pm$ production could show up sharp peaks at $M_{\mu\mu} \simeq m_H$ and $M_{\mu\mu} \simeq m_A$ on top of the background contributions. The resolution would be sufficient to determine the mass of the Higgs bosons, since it is constructed from the muon momenta.

In order to measure the mass of the charged Higgs boson, we propose an analysis using the transverse mass variable. First, we further purify the events by requiring opposite-sign in the muon pair to extract the dimuon which comes from the decay of the neutral Higgs boson. For the same purpose, the cut on the transverse momentum of the dimuon is applied. This cut reduces the significance S slightly, however, it rather enhances the signal-to-background ratio s/b . Such purification of the signal events enables us to see the delicate structure of the transverse mass distribution for the signal events. The transverse mass of the tau-jet and the missing transverse momentum is constructed by

$$M_T = \sqrt{2p_T^{\tau_h} \cdot \cancel{E}_T \cdot (1 - \cos \Delta\phi)}, \quad (12)$$

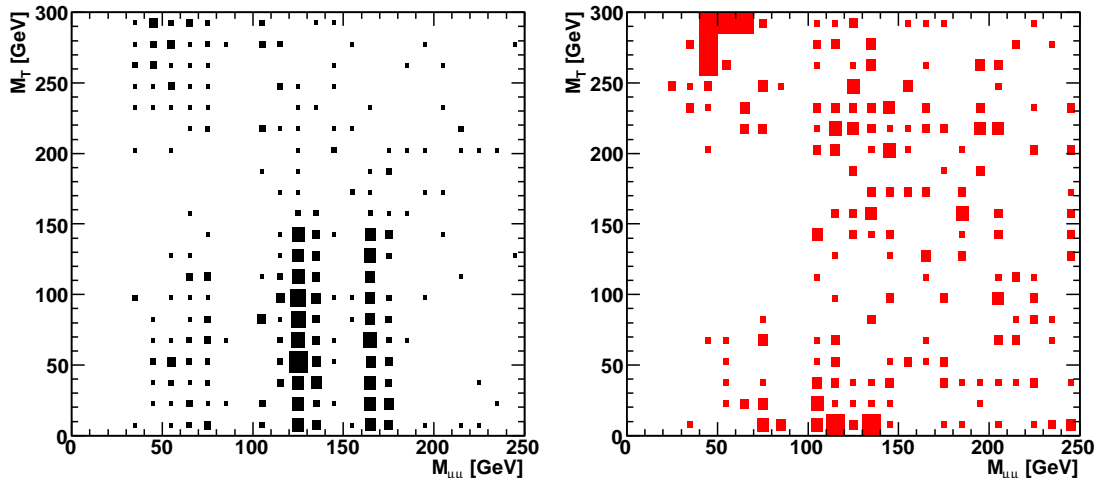


FIG. 10: Two dimensional distributions of the dimuon invariant mass and the transverse mass of the tau-jet and the missing transverse momentum for the signal process (left) and the sum of the background processes (right) in the $2\mu 1\tau_h$ channel after the all selection cuts up to $p_T^{\mu\mu} > 80$ GeV in TABLE VIII. The signal process is simulated with $m_H = 130$ GeV, $m_A = 170$ GeV and $m_{H^\pm} = 150$ GeV.

where $\Delta\phi$ is the difference of azimuthal angles of the tau-jet and the missing transverse momentum.

In FIG. 10, two dimensional distributions of $M_{\mu\mu}$ vs. M_T are shown separately for the signal events (left) and the background events (right). The signal distribution shows two bands in $0 \lesssim M_T \lesssim 150$ GeV at $M_{\mu\mu} \simeq 130$ GeV and 170 GeV. Clearly, these bands indicate the signature of $\phi^0 H^\pm$ production followed by $\phi^0 \rightarrow \mu^+ \mu^-$ and $H^\pm \rightarrow \tau^\pm \nu$ with the hadronic decay of the tau lepton. The transverse mass distribution in each band shows an edge at the mass of the charged Higgs boson. In FIG. 11, we show the transverse mass distributions for the mass window of $|M_{\mu\mu} - m_{\phi^0}| \leq 10$ GeV for $\phi^0 = H$ (left) and $\phi^0 = A$ (right). Both distributions have an edge at $M_T \simeq 150$ GeV, which corresponds to the mass of the charged Higgs boson. However the expected number of events for $L = 100 \text{ fb}^{-1}$ is not large enough. If a sufficient number of events is accumulated, it should be possible to measure the mass of the charged Higgs boson from the position of the edge in the transverse mass distribution around $M_{\mu\mu} \simeq m_H$ and m_A .

Similar channels to the $2\mu 1\tau_h$ channel are 3μ and $2\mu 1e$. We summarize the selection cuts for these process in TABLE IX.

2. Three-lepton channels with two or more tau-jets

Then, we study the three-lepton channels with two or more tau-jets. Similarly to the four-lepton channels with two or more tau-jets, these channels are expected to have large number of events due to the dominant branching ratios into tau leptons. On the other hand, due to the many sources of the missing momentum, namely neutrinos from the decay of the charged Higgs boson and the tau leptons, the reconstruction of the event kinematics is limited.

Here, we present the analysis on the $3\tau_h$ channel and study how the mass information can be

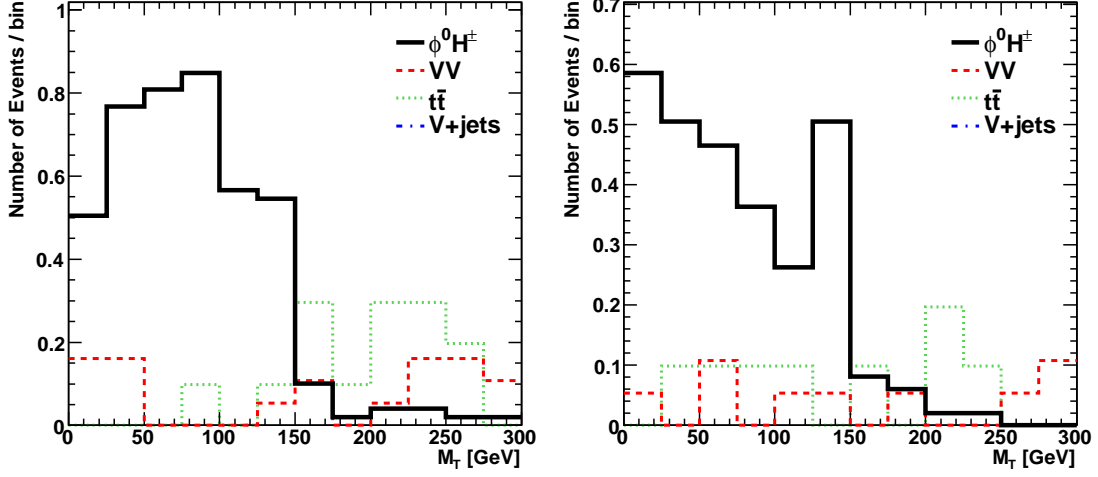


FIG. 11: Distributions of the transverse mass of the tau-jet and the missing transverse momentum with $120 \text{ GeV} < M_{\mu\mu} < 140 \text{ GeV}$ (left) and $160 \text{ GeV} < M_{\mu\mu} < 180 \text{ GeV}$ (right) for the $2\mu 1\tau_h$ channel after the selection cuts. The signal processes is simulated with $m_H = 130 \text{ GeV}$, $m_A = 170 \text{ GeV}$ and $m_{H^\pm} = 150 \text{ GeV}$.

Lepton channels	$2\mu 1\tau_h$		3μ		$2\mu 1e$	
	s/b	(S)	s/b	(S)	s/b	(S)
Pre-selection	445./2330550.	(0.3)	34.1/4214.	(0.5)	81.8/3880.	(1.3)
$p_T^{\tau_h} > 40 \text{ GeV}$	301./465015.	(0.4)	-	(-)	-	(-)
$\cancel{E}_T > 80 \text{ GeV}$	135./3163.	(2.4)	13.9/416.	(0.7)	30.6/385.	(1.5)
$H_T^{\text{jet}} < 30 \text{ GeV}$	73.1/320.	(3.9)	-	(-)	-	(-)
$H_T^{\text{lep}} > 350 \text{ GeV}$	39.7/113.	(3.5)	7.5/122.	(0.7)	14.3/115.	(1.3)
$(m_Z)_{\mu\mu} \pm 10 \text{ GeV}$	36.2/74.4	(3.9)	7.0/67.8	(0.8)	13.2/11.9	(3.3)
O.S. muons	25.3/73.3	(2.8)	-	(-)	9.2/10.0	(2.6)
$p_T^{\mu\mu} > 80 \text{ GeV}$	17.1/41.5	(2.5)	-	(-)	-	(-)
$(m_{\phi^0})_{\mu\mu} \pm 10 \text{ GeV}$	6.1/5.4	(2.3)	3.0/7.7	(1.0)	4.0/1.0	(2.9)

TABLE IX: Summary of event rejection by the selection cuts for the three-lepton channels with two or more muons.

extracted in this channel. In FIG. 12, we show distributions of kinematical variables, $p_T^{\tau_h}$, $p_T^{\tau_h\tau_h}$, \cancel{E}_T , H_T^{jet} and H_T^{lep} . The numbers of the signal and background events are normalized to be unity. Taking into account these distributions, we apply the following selection cuts for the signal and background events;

$$p_T^{\tau_h} > 60 \text{ GeV}, \quad (13a)$$

$$\cancel{E}_T > 80 \text{ GeV}, \quad (13b)$$

$$H_T^{\text{jet}} < 50 \text{ GeV}, \quad (13c)$$

$$H_T^{\text{lep}} > 350 \text{ GeV}. \quad (13d)$$

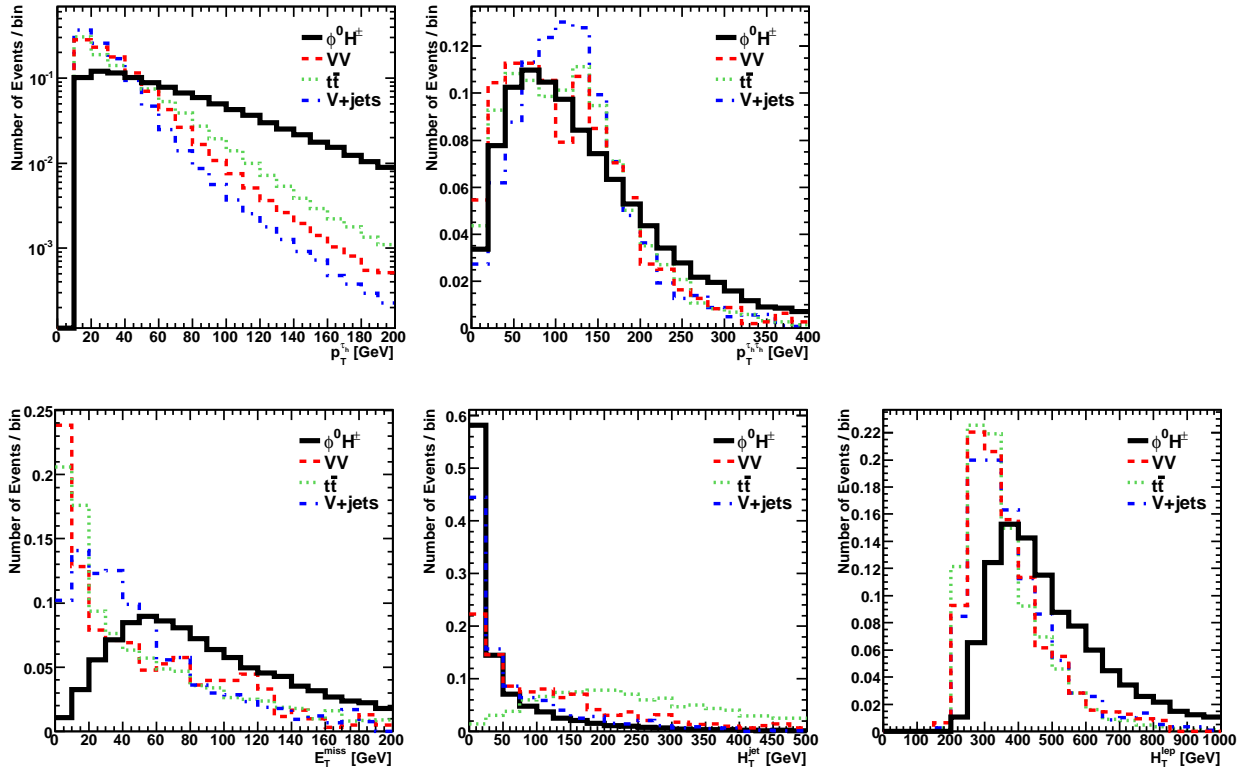


FIG. 12: Distributions of kinematical variables for the $3\tau_h$ channel. Line descriptions follow those in FIG. 1.

$3\tau_h$ event analysis	HA	$\phi^0 H^\pm$	VV	$t\bar{t}$	V +jets	s/b	S (100 fb $^{-1}$)
Pre-selection	710.5	2476.	7069.	42053.	777043.	10^{-3}	3.5
$p_T^{\tau_h} > 60$ GeV	88.4	299.	34.2	341.	1237.	0.2	9.3
$\cancel{E}_T > 80$ GeV	29.3	165.	9.9	89.9	272.	0.5	9.3
$H_T^{\text{jet}} < 50$ GeV	15.8	114.	4.0	4.8	123.	1.0	9.9
$H_T^{\text{lep}} > 350$ GeV	15.0	106.	3.4	3.8	108.	1.0	9.9

TABLE X: Table for background reductions in the $3\tau_h$ channel.

The summary of the results of event reductions is given in TABLE X. After the all cuts, more than a hundred event is expected for the signal processes, while the background events are estimated to be around 120 which is dominated by the V +jets process for $L = 100$ fb $^{-1}$. The expected reach of the significance is close to 10 for $L = 100$ fb $^{-1}$. It may indicate the possibility of an earlier evidence of the signal in this channel. The larger H_T^{lep} cut can be applied to enhance the signal-to-background ratio, which however tends to reduce the significance.

In the left panel in FIG. 13, we plot the invariant mass distributions of the tau-jet pair with opposite charges after the selection cuts for the signal and background processes, where the pair of the two tau-jets is chosen such that it has opposite charges and gives the largest transverse momentum $p_T^{\tau_h\tau_h}$. The $M_{\tau_h\tau_h}$ distribution shows an endpoint behavior at $M_{\tau_h\tau_h} \simeq 170$ GeV which corresponds to the mass of the heavier neutral Higgs boson. Another sharp edge may be able to

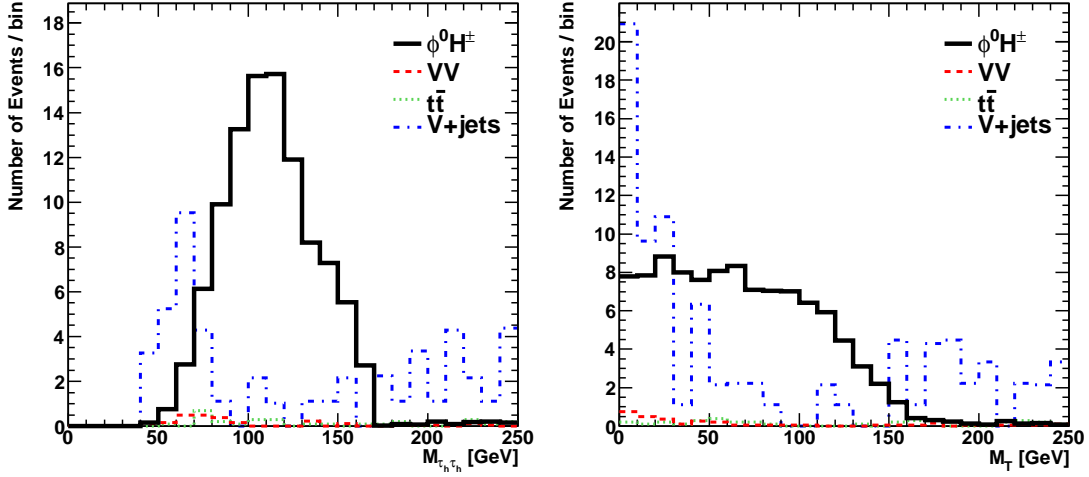


FIG. 13: Distributions of the invariant mass of the tau-jet pair (left) and the transverse mass of the remaining tau-jet and the missing transverse momentum in the $3\tau_h$ channel after the selection cuts. The pairing rule of the tau-jets is explained in the text.

be pinned down at $M_{\tau_h\tau_h} \simeq 130$ GeV the mass of the lighter neutral Higgs boson. In the right panel, distributions of the transverse mass M_T constructed from the remaining tau-jet and the missing transverse momentum using Eq. (12) are shown for the signal and background events after the selection cuts in the $3\tau_h$ channel. The M_T distribution for the signal events vanishes around $M_T \simeq 150$ GeV, however the slope is, in contrast to the $2\mu 1\tau_h$ channel, rather gentle but not seen like an endpoint. This is because there are many sources of the missing momentum in this channel.

In the left panel in FIG. 14, we plot the two dimensional distribution of the invariant mass of the tau-jet pair and the transverse mass in the $3\tau_h$ channel after the selection cuts. In the right panel, the dominant V +jets background events are plotted. The V +jets background events widely distribute in the two dimensional space of $M_{\tau_h\tau_h}$ and M_T . On the other hand, the signal events distribute compactly in the region of $50 \text{ GeV} \lesssim M_{\tau_h\tau_h} \lesssim \max(m_H, m_A)$ and $0 \lesssim M_T \lesssim m_{H^\pm}$. Therefore, if the sufficient number of events is accumulated, we may have an indication of the masses of the charged Higgs boson and the neutral Higgs bosons by catching the border of the signal-event-like distribution.

Similar channels to the $3\tau_h$ channel are $2\tau_h 1\mu$ and $2\tau_h 1e$. We summarize the selection cuts for these processes in TABLE XI. The three-lepton channels with one or less muon or electron suffer large background contributions from the W +jets process, thus the s/b ratio is not so large. However due to the large number of the signal events, the significance S can be large enough. There are also $1\tau_h 1\mu 1e$, $1\tau_h 2e$, $1\mu 2e$ and $3e$ channels. For the reference, we list the summary of reductions of events in TABLE XII.

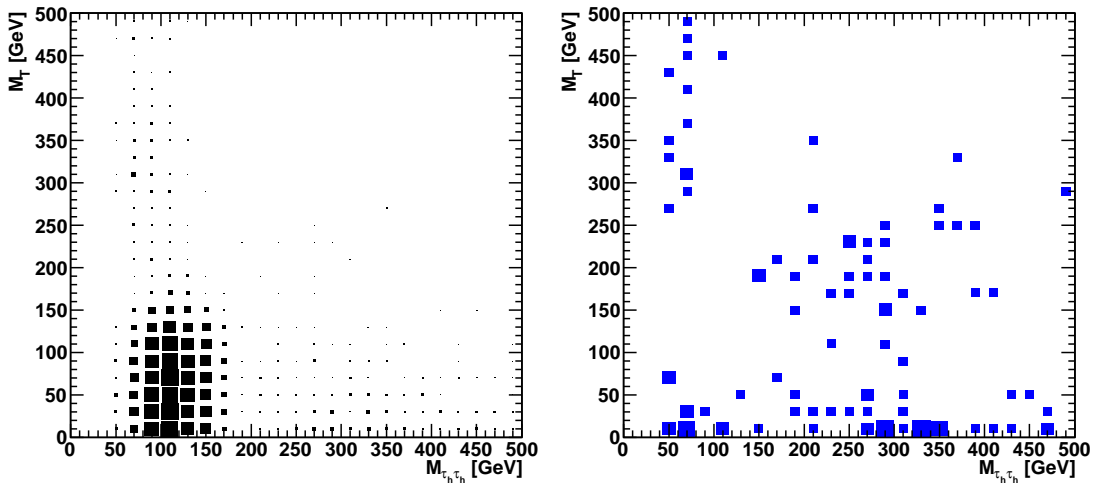


FIG. 14: Two dimensional distributions of the invariant mass of the tau-jet pair versus the transverse mass in the $3\tau_h$ channel after the selection cuts. The left panel is for the signal process, and the right panel is for the background processes. The normalization of the two panels is adjusted.

Lepton channels	$3\tau_h$		$2\tau_h 1\mu$		$2\tau_h 1e$	
	s/b	(S)	s/b	(S)	s/b	(S)
Pre-selection	3186./826165.	(3.5)	2001./622055.	(2.5)	1794./571334.	(2.4)
$p_T^{\tau_h} > 60$ GeV	387./1612.	(9.3)	494./7346.	(5.7)	443./7368.	(5.1)
$\cancel{E}_T > 80$ GeV	194./372.	(9.3)	244./1940.	(5.4)	216./1805.	(5.0)
$H_T^{\text{jet}} < 50$ GeV	129./132.	(9.9)	158./761.	(5.5)	142./738.	(5.1)
$H_T^{\text{lep}} > 350$ GeV	121./116.	(9.9)	124./434.	(5.7)	112./437.	(5.2)

TABLE XI: Summary of event rejection by the selection cuts for the three-lepton channels with two or more tau-jets.

IV. SUMMARY AND DISCUSSIONS

In this section, we present a summary and discussions of our simulation studies, and give discussions for the neutral Higgs pair production at electron-positron linear colliders. Finally, we conclude the paper.

We have studied multi- τ signatures at the LHC in the Type-X THDM. Assuming $\tan\beta \gtrsim 3$, more than 99% of extra Higgs bosons H, A and H^\pm decays into tau leptons. These Higgs bosons can be pair produced in $q\bar{q} \rightarrow HA$ and $q\bar{q}' \rightarrow \phi^0 H^\pm$ processes where $\phi^0 = H, A$, and they produce characteristic multi- τ final states at the LHC. We have focused on the $2\mu 2\tau$ and 4τ states for the pair production of the neutral Higgs bosons, and on the $2\mu 1\tau 1\nu$ and $3\tau 1\nu$ states for the charged Higgs boson associated production followed by the decays of tau leptons into leptons or hadrons. These result in the various four- and three-lepton channels which include tau-jets. We have performed the Monte-Carlo simulation for the signal processes as well as the major background processes, namely $VV, t\bar{t}$ and V +jets processes at the LHC where $V = W, Z$. The realistic tau-jet

Lepton channels	$1\tau_h 1\mu 1e$	$1\tau_h 2e$	$1\mu 2e$	$3e$
	s/b (S)	s/b (S)	s/b (S)	s/b (S)
Pre-selection	738./65150. (2.9)	333./1883890. (0.2)	68.8/3431. (1.2)	20.0/3107. (0.4)
$p_T^{\tau_h} > 40$ GeV	498./17718. (3.7)	226./373858. (0.4)	- (-)	- (-)
$\cancel{E}_T > 80$ GeV	302./4971. (4.2)	97.3/2456. (2.0)	22.7/343. (1.2)	6.7/302. (0.4)
$H_T^{\text{jet}} < 30$ GeV	113./455. (5.1)	52.8/259. (3.2)	- (-)	- (-)
$H_T^{\text{lep}} > 350$ GeV	58.5/128. (4.8)	27.7/94.4 (2.7)	9.1/99.5 (0.9)	2.7/90.7 (0.3)
$(m_Z)_{ee} \pm 10$ GeV	- (-)	24.2/62.8 (2.9)	7.9/11.2 (2.2)	2.2/39.9 (0.3)

TABLE XII: Summary of event rejection by the selection cuts for the rest of three-lepton channels.

tagging procedure is simulated for the final state hadrons. For leptons, the standard acceptance cuts and isolation conditions are considered. Then we have applied the selection cuts to reduce the background contributions for each channel. We here summarize the analysis for the four- and three-lepton channels to probe the pair production of the neutral Higgs bosons and the charged Higgs boson associated production, respectively, in order.

- For the four-lepton channels with two or more muons, the mass of the neutral Higgs bosons can be measured as the peaks in the $M_{\mu\mu}$ distribution. For these events where the dimuon comes from the direct decay of the Higgs boson, the tau lepton momenta can be reconstructable by using the collinear approximation for the rest two leptons out of the four. The two dimensional distribution of the $M_{\mu\mu}$ and the reconstructed $M_{\tau\tau}$, such like shown in FIG. 4, would be a direct test of the neutral Higgs bosons pair production in the Type-X THDM. However, the numbers of the signal events are relatively small due to the small branching ratio of the neutral Higgs bosons into dimuons. The signal-to-background ratio is rather large, thus a clean extraction is possible, if the number of events is sufficient. The information of the branching ratio of the neutral Higgs boson into dimuons can also be extracted.

The detailed analysis is performed for the $2\mu 2\tau_h$ channel, and the summary of the selection cuts for the similar channels is found in TABLES III and IV.

- For the four-lepton channels with two or more tau-jets, a large number of signal events are expected due to the dominant branching ratio of the neutral Higgs bosons into tau leptons. After the selection cuts, both the signal-to-background ratios s/b and the significances S are large, so that the excess can be relatively easily found. On the other hand, the mass determination would only be possible by looking at the kinematical distributions. Searches for the endpoints or bumps in the $M_{\tau_h\tau_h}$ distributions, shown in FIGs. 6 and 7 can indicate the mass of the neutral Higgs bosons, provided the sufficient number of events are accumulated.

The analysis for the $4\tau_h$ channel is presented in detail, and the selection cuts for the similar channels are summarized in TABLES V and VI. For completeness, a summary of the selection cuts for the rest of the four-lepton channels is presented in TABLE VII.

- For the three-lepton channels with two or more muons, the mass of the neutral Higgs bosons can be measured by looking for the peaks in the $M_{\mu\mu}$ distribution. The mass of the charged Higgs boson can be measured as the edge of the distributions of the transverse mass M_T which is constructed from the rest of the three-leptons and the missing transverse momentum. By focusing on the events with $M_{\mu\mu} \simeq m_H$ or m_A , an edge can be enhanced such as shown in FIG. 11, which corresponds to the charged Higgs boson mass. Due to the large background contribution from the V +jets process, the s/b ratio is small.

The analysis for the $2\mu 1\tau_h$ channel is presented in detail, and the selection cuts for the the similar channels are summarized in TABLES VIII and IX.

- For the three-lepton channels with two or more tau-jets, a large number of signal events is expected due to the dominant branching ratio of Higgs bosons into tau leptons. However due to the large background contribution from the V +jets process, the s/b ratio is rather small even after the selection cuts. Using the two dimensional distributions of $M_{\tau_h\tau_h}$ and the transverse mass M_T , as shown in FIG. 14, the information of the mass of the Higgs bosons can be obtained.

The analysis for the $3\tau_h$ channel is presented in detail, and the selection cuts for the similar channels are summarized in TABLES X and XI. For completeness, a summary of the selection cuts for the rest of the three-lepton channels is presented in TABLE XII.

We have shown that the characteristic excess from the production and the decay of the lepton-specific Higgs bosons can be observed in the various four- and three-lepton channels on top of the SM contributions at the LHC. However, on the other hand, the determination of the mass of the Higgs bosons seems not to be feasible with the integrated luminosity of $L = 100 \text{ fb}^{-1}$, although we have shown the various methods in various channels. The measurement of the branching ratio of the neutral Higgs bosons into dimuons which we have examined in the $2\mu 2\tau_h$ channel, also requires the number of events more than the expected for $L = 100 \text{ fb}^{-1}$. These measurement should be achieved with the running of the luminosity upgraded LHC in future [46]. With the luminosity of an order of thousand inverse fb, it is promising to measure the mass of the neutral and charged Higgs bosons as well as the branching ratio of the neutral Higgs boson into dimuons.

We here briefly comment on the search potential for the lepton-specific Higgs bosons at the International Linear Collider (ILC) or the Compact Linear Collider (CLIC). The neutral Higgs bosons can be pair produced via the $e^+e^- \rightarrow HA$ process, and their decay produces four- τ states predominantly. Through the leptonic and hadronic decay of the tau leptons, the signatures are four-lepton channels including tau-jets, as we have studied for the hadron colliders. At e^+e^- colliders, four momenta of the four tau leptons can be solved by applying the collinear approximation to all the four decay products of the tau leptons [25, 47], because the missing four momentum can be reconstructed by the energy momentum conservation. In Ref. [48], it is shown that clear peaks can be observed in the one dimensional and two dimensional distributions for the invariant masses of the reconstructed tau lepton pairs.

In conclusion, we have studied the multi- τ signatures at the LHC in the THDM with lepton-specific Yukawa interactions. At the LHC, such Higgs bosons can be pair produced via the weak boson mediated processes, and predominantly they decay into multi- τ states. Although the event reconstruction is limited due to the missing energies from the decays of the tau leptons, it is possible to discriminate the signal events from the background events by requiring the high multiplicity of the leptons and the tau-jets with appropriate kinematical cuts in various four and three-lepton channels. The mass of the Higgs bosons can be measured by using the invariant mass distributions of the dimuon which comes from the direct decay of the neutral Higgs bosons as well as the endpoint analysis for the distributions of the invariant mass of the tau-jets and the transverse mass, if sufficiently large integrated luminosity is accumulated. We have found that measurements of multi- τ final states at hadron colliders can be a useful probe of the properties of the Higgs bosons in the lepton-specific models.

Acknowledgments

We thank S. Odaka and the KEK Atlas group for providing us and managing computing environment to execute the Monte-Carlo simulation in this work. The work of S.K. was supported in part by Grant-in-Aid for Scientific Research, Japan Society for the Promotion of Science (JSPS), Nos. 22244031 and 23104006. The work of K.T. was supported in part by the National Science Council of Taiwan under Grant No. NSC 100-2811-M-002-090. The work of H.Y. was supported in part by the National Science Council of Taiwan under Grant No. NSC 100-2119-M-002-001. K.T. and H.Y. would like to thank the theoretical physics group in university of Toyama for their warm hospitality.

Appendix A: Tau-jet tagging efficiency

In this appendix, we present a rough estimation of the tau-jet tagging efficiency and the mis-tagging probabilities for the non-tau jet in our tau-jet tagging procedure defined in the main text. We neglect the η and p_T dependences of the efficiency as well as the mis-tagging probability. This information may be useful to estimate the variation of our results by changing the conditions of tau-jet tagging, and also to compare with the actual experimental situation at the LHC.

The tau-jet tagging efficiency is estimated from the signal events in $4\tau_h$ and $3\tau_h$ channels from HA production and $\phi^0 H^\pm$ production, respectively. In the $4\tau_h$ channel, the number of events after the pre-selection for the signal events is ~ 320 for the integrated luminosity of 100 fb^{-1} (see TABLE V). On the other hand, the expected number of the 4τ final-state is $50 [\text{fb}] \times 100 [\text{fb}^{-1}] \sim 5000$. From this, the probability of finding the tau-jet per decay of one tau lepton is estimated to be $(320/5000)^{1/4} \sim 0.50$. This can be interpreted as the product of the branching ratio of the hadronic decay of tau leptons, the acceptance ratio for $|\eta| < 2.5$ and $p_T > 10 \text{ GeV}$ and also the tau-jet tagging efficiency. By using the branching ratio of hadronic decays of tau leptons which is about

65% [1], the multiplication of the the acceptance ratio and tau-jet tagging efficiency is estimated to be ~ 0.77 . Further separation of the two factors is too confusing to us. For confirmation we have checked that the obtained value gives roughly correct number of the signal events from $\phi^0 H^\pm$ production in the $3\tau_h$ channel by $200 \text{ [fb]} \times 100 \text{ [fb}^{-1}] \times (0.50)^3 \sim 2500$ (compare with the number of signal events from $\phi^0 H^\pm$ production after the pre-selection in TABLE X).

The mis-tagging probability for non-tau jets is estimated for the V +jets events in the $2\mu 2\tau_h$ and $2\mu 1\tau_h$ channels. The numbers of events from the V +jets production after the pre-selection are $2.9 \cdot 10^4$ and $2.3 \cdot 10^6$ for the $2\mu 2\tau_h$ and $2\mu 1\tau_h$ channels, respectively, where here the requirement of the zero charge-sum is not imposed in the former channel. For our V +jets events, the fraction of the events which exclusively contain one (two) primal jet(s) with $|\eta| < 2.5$ and $p_T > 10 \text{ GeV}$ is found to be 0.09 (0.01). The expected number of events for the $\mu^+ \mu^- jj$ final-state from the V +jets process is $30 \text{ [nb]} \times 100 \text{ [fb}^{-1}] \times 0.33 \times 0.01 \sim 10^7$, where a factor of 0.33 comes from the fraction of the dimuon final-state in the leptonic Z -boson decays. Thus the mis-tagging probability per jet is estimated to be $\sqrt{2.9 \cdot 10^4 / 10^7} \sim 0.05$. The same probability is estimated for the $2\mu 1\tau_h$ channel as $2.3 \cdot 10^6 / (10^9 \times 0.09) \sim 0.03$. Thus the mis-tagging probability per jet for the V +jets process should be a few percent in our simulation.

Similarly the mis-tagging probability for the $t\bar{t}$ events can be estimated by using the dimuon decay of the $t\bar{t}$ events. For the $t\bar{t}$ events, one or two jets are expected to be originated from the b quark, and the mis-tagging probability for such jets may be different from that for the light-flavor jets. However, we ignore the difference of the mis-tagging probabilities by the flavor of jets. The number of events for the dimuon decay mode of our $t\bar{t}$ events is given as $493 \text{ [pb]} \times 100 \text{ [fb}^{-1}] \times (0.107)^2 \sim 5.6 \cdot 10^5$. For the dimuon decay channel in our $t\bar{t}$ events, an average number of the primal jet with $|\eta| < 2.5$ and $p_T > 10 \text{ GeV}$ is $\sum_{n=1} r_n n \sim 3.6$ where r_n is the fraction of events with n primal-jets which satisfies $\sum_{n=0} r_n = 1$, and also an average number of the combination of the two primal jets is $\sum_{n=2} r_n \binom{n}{2} \sim 5.8$. By removing the requirement of zero charge-sum of the four-lepton at the pre-selection in the $2\mu 2\tau_h$ channel, the number of events after the pre-selection is ~ 800 , thus the mis-tagging probability is estimated to be $\sqrt{800 / (5.6 \cdot 10^5 \times 5.8)} \sim 0.02$. On the other hand, for the $2\mu 1\tau_h$ channel, the mis-tagging probability is estimated to be $2.3 \cdot 10^4 / (5.6 \cdot 10^5 \times 3.6) \sim 0.01$. Thus the mis-tagging probability per jet for the $t\bar{t}$ process should be also a few percent. The smaller mis-tagging probability for the $t\bar{t}$ process by our rough estimation may be due to the large QCD activity in the $t\bar{t}$ events which could prevent the isolation of the charged tracks in the tau-jets.

One may be able to reduce the mis-tagging probability with minor loss of tagging efficiency, e.g., by using only the 1-prong (or 3-prong) decay mode of tau leptons and/or by applying more tight tagging conditions.

[1] K. Nakamura *et al.* [Particle Data Group Collaboration], J. Phys. GG **37**, 075021 (2010).

[2] G. Aad [ATLAS Collaboration], arXiv:1110.2693 [hep-ex].

[3] The ATLAS Collaboration, Report No. ATLAS-CONF-2011-022; The CMS Collaboration, Report No. CMS-PAS-EXO-11-054.

- [4] R. Barate *et al.* [LEP Working Group for Higgs boson searches and ALEPH and DELPHI and L3 and OPAL Collaborations], Phys. Lett. B **565**, 61 (2003).
- [5] The ATLAS Collaboration, Report No. ATLAS-CONF-2011-135, 2011; The CMS Collaboration, Report No. CMS-PAS-HIG-11-022, 2011.
- [6] The CDF, D0 Collaborations, the Tevatron New Phenomena, Higgs Working Group, Report No. FERMILAB-CONF-11-354-E, 2011.
- [7] S. L. Glashow and S. Weinberg, Phys. Rev. D **15**, 1958 (1977).
- [8] V. D. Barger, J. L. Hewett and R. J. N. Phillips, Phys. Rev. D **41**, 3421 (1990); Y. Grossman, Nucl. Phys. B **426**, 355 (1994).
- [9] M. Aoki, S. Kanemura, K. Tsumura and K. Yagyu, Phys. Rev. D **80**, 015017 (2009).
- [10] V. Barger, H. E. Logan and G. Shaughnessy, Phys. Rev. D **79**, 115018 (2009); S. Su and B. Thomas, Phys. Rev. D **79**, 095014 (2009); H. E. Logan and D. MacLennan, Phys. Rev. D **79**, 115022 (2009).
- [11] E. Ma, Mod. Phys. Lett. A **17**, 535 (2002); E. Ma and D. P. Roy, Nucl. Phys. B **644**, 290 (2002).
- [12] M. Aoki, S. Kanemura and O. Seto, Phys. Rev. Lett. **102**, 051805 (2009); Phys. Rev. D **80**, 033007 (2009); M. Aoki, S. Kanemura and K. Yagyu, Phys. Rev. D **83**, 075016 (2011).
- [13] H. -S. Goh, L. J. Hall and P. Kumar, JHEP **0905**, 097 (2009).
- [14] D. L. Rainwater, D. Zeppenfeld, K. Hagiwara, Phys. Rev. **D59**, 014037 (1998).
- [15] B. K. Bullock, K. Hagiwara, A. D. Martin, Phys. Rev. Lett. **67**, 3055-3057 (1991); Phys. Lett. **B273**, 501-504 (1991); Nucl. Phys. **B395**, 499-533 (1993).
- [16] J. F. Gunion, H. E. Haber, G. Kane and S. Dawson, The Higgs Hunter's Guide (Frontiers in Physics series, Addison-Wesley, Reading, MA, 1990).
- [17] A. Djouadi, Phys. Rept. **459**, 1 (2008).
- [18] J. F. Gunion, H. E. Haber, Nucl. Phys. **B272**, 1 (1986); Nucl. Phys. **B278**, 449 (1986).
- [19] S. Kanemura, Y. Okada, E. Senaha, C. -P. Yuan, Phys. Rev. **D70**, 115002 (2004).
- [20] H. M. Georgi, S. L. Glashow, M. E. Machacek and D. V. Nanopoulos, Phys. Rev. Lett. **40**, 692 (1978).
- [21] Z. Kunszt, Nucl. Phys. B **247**, 339 (1984); J. F. Gunion, H. E. Haber, F. E. Paige, W. -K. Tung and S. S. D. Willenbrock, Nucl. Phys. B **294**, 621 (1987); S. Dittmaier, M. Kramer, 1 and M. Spira, Phys. Rev. D **70**, 074010 (2004); S. Dawson, C. B. Jackson, L. Reina and D. Wackerroth, Phys. Rev. D **69**, 074027 (2004).
- [22] S. Kanemura and C. P. Yuan, Phys. Lett. B **530**, 188 (2002); A. G. Akeroyd, Phys. Rev. D **68**, 077701 (2003); Q. H. Cao, S. Kanemura and C. P. Yuan, Phys. Rev. D **69**, 075008 (2004); A. Belyaev, Q. H. Cao, D. Nomura, K. Tobe and C. P. Yuan, Phys. Rev. Lett. **100**, 061801 (2008).
- [23] D. Benjamin *et al.* [Tevatron New Phenomena & Higgs Working Group Collaboration], arXiv:1003.3363 [hep-ex].
- [24] S. Chatrchyan *et al.* [CMS Collaboration], Phys. Rev. Lett. **106**, 231801 (2011).
- [25] S. Schael *et al.* [LEP Working Group for Higgs boson searches and ALEPH and DELPHI and L3 and OPAL Collaborations], Eur. Phys. J. C **47**, 547 (2006)
- [26] A. Heister *et al.* [ALEPH Collaboration], Phys. Lett. **B543**, 1-13 (2002).
- [27] M. Ciuchini, E. Franco, G. Martinelli, L. Reina, L. Silvestrini, Phys. Lett. **B334** , 137-144 (1994); M. Ciuchini, G. Degrassi, P. Gambino, G. F. Giudice, Nucl. Phys. **B527** , 21-43 (1998); F. Borzumati, C. Greub, Phys. Rev. **D58** , 074004 (1998); P. Gambino, M. Misiak, Nucl. Phys. **B611** , 338-366 (2001).
- [28] M. Misiak, H. M. Asatrian, K. Bieri, M. Czakon, A. Czarnecki, T. Ewerth, A. Ferroglia, P. Gambino *et al.*, Phys. Rev. Lett. **98** , 022002 (2007).
- [29] W. -S. Hou, Phys. Rev. **D48** , 2342-2344 (1993); Y. Grossman, Z. Ligeti, Phys. Lett. **B332** , 373-380 (1994); Y. Grossman, H. E. Haber, Y. Nir, Phys. Lett. **B357** , 630-636 (1995).

- [30] A. A. Barrientos Bendezu and B. A. Kniehl, Nucl. Phys. B **568**, 305 (2000); O. Brein, W. Hollik, Eur. Phys. J. **C13**, 175-184 (2000); S. Moretti, J. Phys. G **28**, 2567 (2002); A. Alves and T. Plehn, Phys. Rev. D **71**, 115014 (2005).
- [31] T. Plehn, Phys. Rev. D **67**, 014018 (2003); E. L. Berger, T. Han, J. Jiang and T. Plehn, Phys. Rev. D **71**, 115012 (2005).
- [32] A. A. Barrientos Bendezu and B. A. Kniehl, Phys. Rev. D **59**, 015009 (1999); O. Brein, W. Hollik and S. Kanemura, Phys. Rev. D **63**, 095001 (2001); E. Asakawa, O. Brein and S. Kanemura, Phys. Rev. D **72**, 055017 (2005); D. Eriksson, S. Hesselbach and J. Rathsmann, Eur. Phys. J. C **53**, 267 (2008).
- [33] W. Hollik, T. Sack, Phys. Lett. **B284**, 427-430 (1992).
- [34] M. Krawczyk, D. Temes, Eur. Phys. J. **C44**, 435-446 (2005).
- [35] A. G. Akeroyd, Phys. Lett. **B368**, 89-95 (1996); J. Phys. G **G24**, 1983-1994 (1998).
- [36] J. Alwall, M. Herquet, F. Maltoni, O. Mattelaer, T. Stelzer, JHEP **1106**, 128 (2011).
- [37] S. Jadach, Z. Was, R. Decker and J. H. Kuhn, Comput. Phys. Commun. **76**, 361 (1993).
- [38] T. Sjostrand, S. Mrenna, P. Z. Skands, JHEP **0605**, 026 (2006).
- [39] J. Pumplin, D. R. Stump, J. Huston, H. L. Lai, P. M. Nadolsky and W. K. Tung, JHEP **0207**, 012 (2002).
- [40] D. Toussaint, Phys. Rev. D **18**, 1626 (1978); S. Bertolini, Nucl. Phys. B **272**, 77 (1986).
- [41] S. Kanemura, Y. Okada, H. Taniguchi and K. Tsumura, Phys. Lett. B **704**, 303 (2011).
- [42] M. Cacciari, G. P. Salam and G. Soyez, JHEP **0804**, 063 (2008).
- [43] M. Cacciari, G. P. Salam, Phys. Lett. **B641**, 57-61 (2006); M. Cacciari, G.P. Salam and G. Soyez, <http://fastjet.fr/>.
- [44] G. Aad *et al.* [ATLAS Collaboration], arXiv:1108.2016 [hep-ex], Report No. ATLAS-CONF-2011-077.
- [45] The CMS Collaboration J. Phys. G **34**, 995 (2007).
- [46] F. Gianotti *et al.*, Eur. Phys. J. C **39**, 293 (2005); M. Mangano, Contemp. Phys. **51**, 211 (2010).
- [47] J. Abdallah *et al.* [DELPHI Collaboration], Phys. Lett. B **552**, 127 (2003).
- [48] S. Kanemura, K. Tsumura, H. Yokoya, Presentation given by KT at the International Workshop on Future Linear Colliders 2011 (LCWS2011), 26-30, September, 2011, Granada, Spain.